Journal of Applied Physics REVIEW pubs.aip.org/aip/jap

Recent advances toward damage-tolerant 3D-printed titanium alloys: Alloy design perspective

Cite as: J. Appl. Phys. **139**, 040701 (2026); doi: 10.1063/5.0287936
Submitted: 27 June 2025 · Accepted: 26 December 2025 ·
Published Online: 26 January 2026

Saeid Alipour,[1,2,a)] Arezoo Emdadi,[1] and Ju Li[2,a)]

AFFILIATIONS

[1]Department of Materials Science and Engineering, Missouri University of Science and Technology, Rolla, Missouri 65409, USA
[2]Department of Materials Science and Engineering and Department of Nuclear Science and Engineering, Massachusetts Institute of Technology, Cambridge, Massachusetts 02139, USA

Note: This paper is part of the Special Topic on Transformative Frontiers in Additive Manufacturing
[a)]**Authors to whom correspondence should be addressed:** liju@mit.edu and saeid250@mit.edu

ABSTRACT

Twenty-year uninterrupted endeavor of titanium alloys printing has opened up a new paradigm in metal additive manufacturing (AM) to fabricate engineering components with required strength–density–corrosion combinations. Despite the remarkable advances in titanium AM, controlling the grain structure to print the parts with engineered microstructures, tailored mechanical properties, and minimum anomalies remains challenging. Numerous approaches have been implemented to address this challenge, such as printing parameter control, post-AM heat treatments, and thermomechanical processing. In addition to the aforementioned conventional approaches, novel techniques have been proposed that require employing hybrid manufacturing or developing the printer itself. One of the novel pathways in developing damage-tolerant 3D-printed titanium alloys lies in modifying or re-designing the alloy composition. This pathway strives to exploit the unique solidification conditions of AM processes, which are typically different than conventional manufacturing techniques such as casting, forging, and rolling. Hence, this review paper aims to scrutinize the pathway toward Ti alloy modification/re-designing, which can lead to damage-tolerant Ti parts being printed via various AM methods, targeting performance-critical applications.

I. INTRODUCTION

According to ASTM F2792,[1] 3D printing is the fabrication of objects through the deposition of a material using a print head, nozzle, or another printer technology. The 3D printing term often used synonymously with additive manufacturing (AM) which is defined as a process of joining materials to make objects from 3D model data, usually layer upon layer, as opposed to subtractive manufacturing methodologies. Since the emergence of AM, there have been unprecedented opportunities in the production of metal components for the vast majority of applications, such as aerospace, energy, automotive, and biomedical, to name but a few.[2–7] The preeminent reason for this lies in the layer-wise production manner of printed parts, thereby enabling the production of engineering components with a near-net shape and unique intricate geometries, which commonly cannot be achieved with conventional manufacturing techniques such as casting, forging, rolling, and machining.[8] Among the various engineering alloys, titanium (Ti) alloys have opened up a new area in AM due to their high strength, low density, excellent corrosion resistance, and acceptable biocompatibility.[9–11] Hence, within the last twenty years, there has been an uninterrupted endeavor to transition research efforts on the AM of Ti alloys by addressing phase heterogeneities and potential anomalies, employing them for practical engineering applications. Fuel nozzles, propellers, low-pressure turbines, wing brackets, landing gear assembly, pressure bulkhead, surgical implants, and joint replacements are only a few examples of the additively manufactured (AMed) Ti components that are currently being used in existing performance-critical applications.[12–15] Figure 1 shows some of the examples of emerging applications of AM Ti alloys

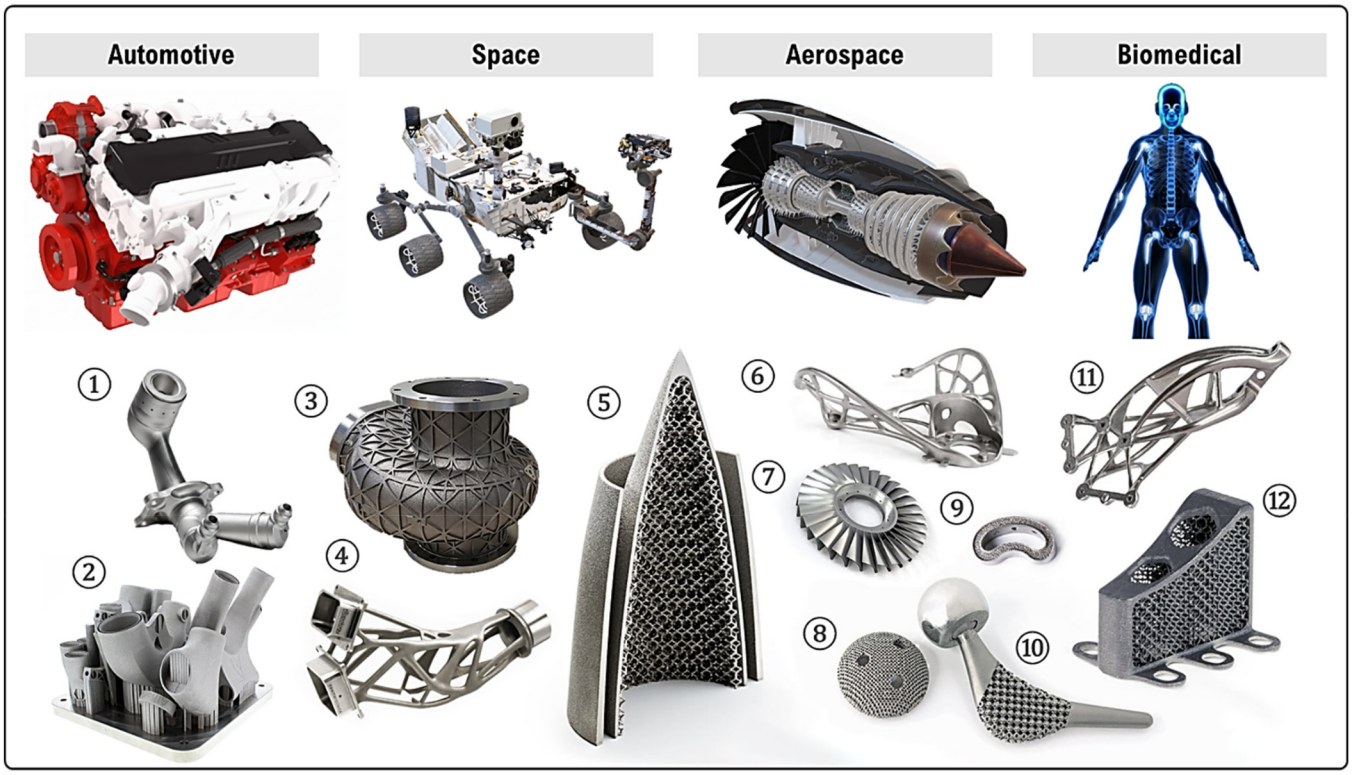

FIG. 1. Emerging applications of AM Ti alloys in various engineering disciplines, such as automotive, space exploration and rocket propulsions, aerospace and turbines, as well as biomedical load-bearing implants. Some of the AM Ti components for existing performance-critical applications: ①: fuel nozzle by GE Aviation, ②: Ti lugs by Atherton Cycles, ③: turbopump casing and ④: spacecraft bracket by Zenith Tecnica, ⑤: rocket tip by Arcam, ⑥: topologically optimized satellite bracket by 3D Systems and Thales Alenia Space, ⑦: impeller by Sciaky, ⑧: acetabular cup by GE Additive, ⑨: surgical spinal implant by Zenith Tecnica, ⑩: hip joint by GE Additive, ⑪: Liebherr trolley support bracket by EOS and Liebherr, ⑫: lattice implant by 3D systems.

in various engineering disciplines such as automotive, space, aerospace, and biomedical applications.

However, the current AMed Ti alloys usually require additional post-treatments, such as stress relief and annealing, to eliminate residual stresses induced by intrinsic heating and cooling cycles during the printing process.[16–18] Furthermore, hot isostatic pressing (HIP) is one of the other post-processing treatments that is employed in metal AMed parts to decrease the residual anomalies (i.e., lack of fusion defects and porosity) and, at the same time, control the microstructure with the concurrent heat treatment.[19] Although the aforementioned post-treatments can help reduce some of the microstructural heterogeneities and process-induced anomalies to some extent, they might not be thoroughly effective in producing components with desired microstructural and mechanical properties because of the potential grain coarsening, undesired phase transformations, and inability to eliminate various types of defects. Besides, due to the layer-by-layer building process in AM, the newly solidified grains would favorably follow the pre-existing grain orientation in the previous layer; this results in columnar grains spanning over multiple layers in the building direction.[20,21] In the majority of cases, controlling the printing parameters, including laser power, scan speed, and layer thickness, may not fully mitigate the columnar grain growth, as adjusting the printing parameters may result in porosity, lack of fusion, or other types of anomalies, on the other hand.[22] Columnar grains in the microstructure of AMed components are generally unfavorable owing to the anisotropy they induce in the mechanical performance. Therefore, balancing the microstructure–density–performance to manufacture reliable engineering parts appears to be a challenging yet achievable task.

Within the past few years, there has been a great deal of effort in the development of strong and ductile 3D-printed Ti alloys through applying novel approaches that primarily stem from either metallurgical fundamentals or printer modifications.[23–28] High-intensity acoustic vibration,[29,30] hybridizing microstructures,[31,32] *in situ* heat treatment,[33,34] thermo-hydrogen refinement of microstructures,[35,36] forced inter-pass cooling,[37,38] *in situ* peening/rolling,[39,40] deliberately introducing lack of fusion defects with subsequent hot isostatic pressing[19] are some of the proposed approaches in the literature for Ti alloys. Nevertheless, most proposed approaches require 3D printer modifications or additional tools that locate them in the hybrid manufacturing category. Among the proposed approaches, however,

modification of chemical composition and inoculation of Ti alloy have garnered significant attention in AM.[41–43] This emerging interest is mainly ascribed to the unique solidification conditions of AMed alloys, including non-equilibrium conditions, as well as completely different thermal gradients and cooling rates compared to the conventionally manufactured ones, leading to a distinctive microstructure unlike cast and wrought microstructures. This motivation for controlling the microstructure through alloy modification or alloy re-designing also stems from the idea that existing Ti alloy compositions (e.g., Ti-6Al-4V, Ti-6Al-2Sn-4Zr-2Mo, Ti-5Al-5Mo-5V-3Cr) are historically designed and well-crafted for conventional manufacturing techniques like casting with subsequent heat treatments or thermomechanical processes.[44–46] Therefore, the emerging research is being intended for re-designing the alloy composition for AM, resulting in engineered microstructures and excellent mechanical properties. This review paper aims to provide insights into the various proposed approaches, with the focus of alloys design that can be employed for producing 3D-printed Ti alloys with unique mechanical performance.

II. TITANIUM AND TITANIUM ALLOYS: CLASSIFICATION AND PHASES

Based on their compositional balance, which can be accurately determined with the molybdenum equivalent (Mo_{eq}) and aluminum equivalent (Al_{eq}), titanium alloys can fall into α, near-α, α + β, near-β/metastable-β, and fully-β classes.[47] The α (alpha) and β (beta) phases are two different crystal structures of titanium: α is a hexagonal close-packed (HCP) structure stable at low temperatures, whereas β is a body-centered cubic (BCC) structure stable at high temperatures (i.e., above ∼880 °C). These equivalencies are empirical measures of the combined effect of α-stabilizing and β-stabilizing elements, respectively, providing a simplified yet effective approach for conveying phase stability and resulting microstructure of the Ti alloy. The mechanical performance of the Ti alloy, in turn, can be defined by the Mo_{eq} and Al_{eq} values obtained from the relative ratios of α and β phases at room temperature [Fig. 2(a)]. Every type of alloy defines its unique properties via its phase composition and microstructure. β alloys, defined by low Al_{eq} and high Mo_{eq}, are noted for their favorable cold formability and increased strength post-aging, whereas α alloys, defined by high Al_{eq} and low Mo_{eq}, show outstanding weldability and resistance to high-temperature creep.[48] With their balance between phases and flexibility for numerous uses, the α + β alloys offer strength, ductility, and fatigue resistance. However, near-α and near-β alloys show intermediate properties resulting from specific alloying components and thermal treatments. Therefore, classifying Ti alloys based on Mo_{eq} and Al_{eq} is a necessary step in alloy design and selection. Although Mo_{eq} and Al_{eq} offer valuable direction, their oversimplified models ignore the role of phase transitions or processing factors.[49] Hence, Mo_{eq} and Al_{eq} remain basic ideas for understanding the relationship between alloy composition, microstructure, and characteristics in Ti alloys, even if sophisticated simulation approaches are progressively used for enhanced phase prediction.

The microstructural evolution of β-isomorphous (or monotectoid) Ti alloys is defined by the phase transitions occurring during cooling from the elevated-temperature β phase region. These transitions could induce either martensite or equilibrium phases like α and β, depending on the alloy composition and cooling rate.[8] A phase diagram of Ti in Fig. 2(b) reveals several paths for microstructural development together with the ranges of temperature and composition in which certain phases are stable. Comprehending these modifications and cooling rate helps one to control the final microstructure and resultant properties. While intermediate cooling speeds can produce Widmanstätten α, gradual cooling helps the equilibrium α and β phases to form.[50] Widmanstätten is a distinct microstructure formed in Ti alloys with higher cooling rates, characterized by lath-like or acicular colonies of the α phase that grow within prior β grains. Fast cooling may interrupt diffusion and induce a martensitic transition, producing a brittle microstructure. The order of cooling rates for each Ti alloy is specifically determined. As the phase diagram shows, the martensite start (M_s) temperature defines the point below which the martensitic transformation occurs. The ability to regulate the cooling rate helps one to customize the microstructure to acquire particular mechanical characteristics.[51] In addition, the microstructure and mechanical properties of β-isomorphous Ti alloys are improved using heat treatment methods, including aging and solution treatment. Aging facilitates the precipitation of small α particles inside the β matrix, hence enhancing strength; nevertheless, the solution treatment (i.e., heating the alloy to the β phase region) leads to the dissolution of secondary phases. One can design the microstructure for certain uses by carefully controlling the temperature and duration of these heat treatments, therefore attaining a balance among strength, ductility, and other important performance criteria.

Temperature and the presence of β-stabilizing elements greatly influence the microstructure of Ti alloys, a fundamental determinant of their mechanical characteristics. An effective tool for clarifying microstructural variations, displaying a large variety of morphologies, phase distributions, and grain sizes reachable by controlled processing as shown in Fig. 2(c), the continuous cooling transformation (CCT) diagram of Ti-6Al-4V. Ti alloy properties can be tailored to fulfill specific needs for different uses utilizing intentional element modification. Control of Ti alloys' phase transitions and microstructure depends on α- and β-stabilizers. Increasing the quantities of elements including Mo, V, Nb, or Ta will help to promote the β phase development and reduce the β transus temperature.[52] The resulting microstructure could range from totally β structures in alloys with significant β-stabilizer content to equiaxed α grains in alloys with low β-stabilizer content. Furthermore, significantly altering the phase distribution and shape are heat treatment techniques, including annealing, solution treatment, and aging done at different temperatures.[53] Among the microstructures are martensite, equiaxed α, Widmanstätten α, bi-modal α + β, retained β, and grain boundary α, very microstructure exhibits unique characteristics that determine the alloy's general mechanical performance. Knowing how microstructure, processing variables, and features interact can help design Ti alloys with critical-performance applications.

III. NECESSITY TO MOVE FROM THE CONVENTIONAL PSP APPROACH TO NOVEL FPSP[2]

Within the past few years, the data-driven frameworks have been established and implemented for the design of novel alloys for

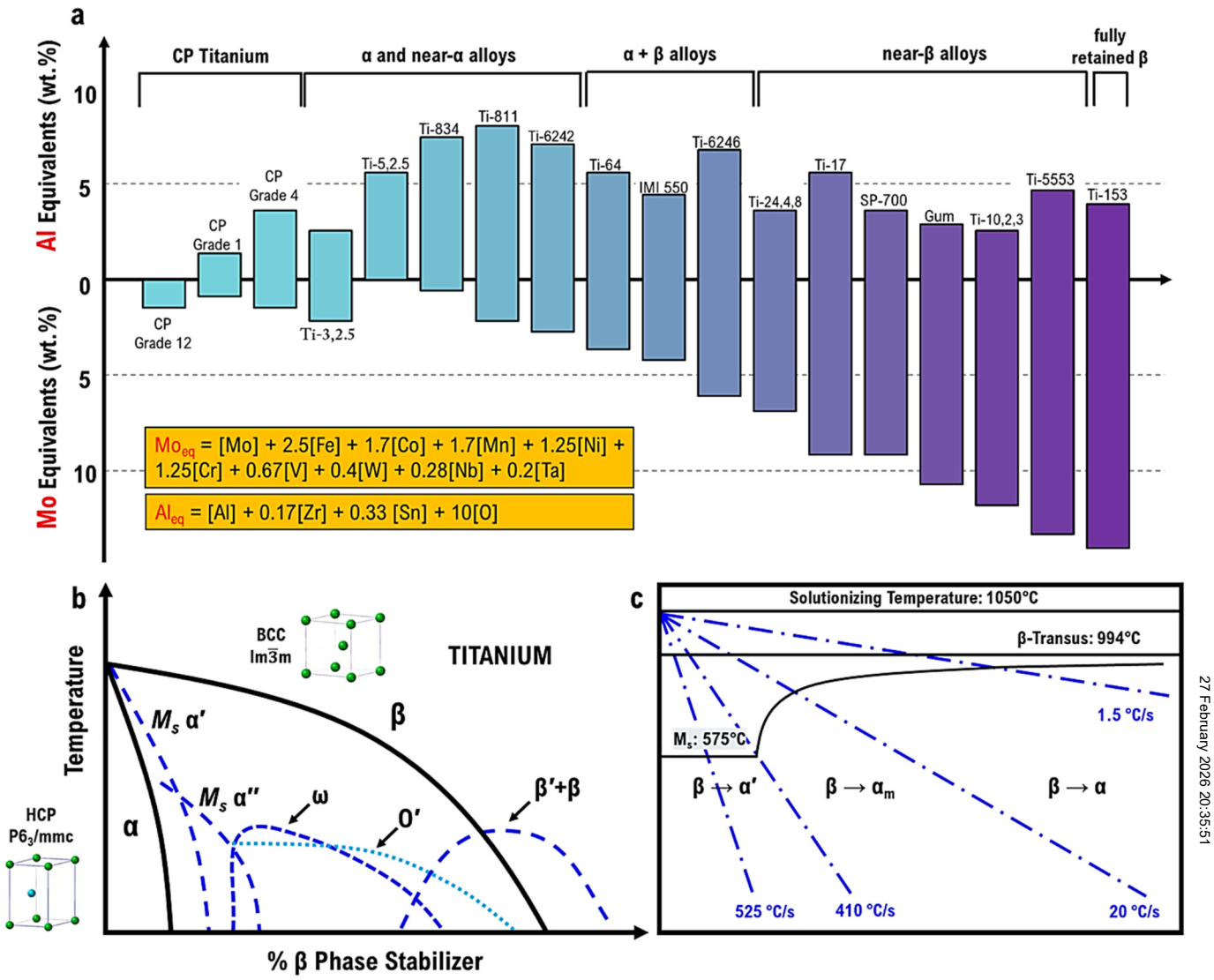

FIG. 2. (a) Classification of various types of Ti alloys according to the molybdenum equivalent (Mo_{eq}) and aluminum equivalent (Al_{eq}). Based on the values for Mo_{eq} and Al_{eq}, Ti alloys are classified as α and near-α, α + β, near-β/metastable-β, and fully-β alloys. (b) Phase diagram illustrating significant equilibrium and metastable phases in Ti for a β-isomorphous (or monotectoid) alloy. Equilibrium phase borders are indicated in bold, while dotted lines represent metastable phase boundaries, (c) CCT diagram for Ti-6Al-4V alloy[54] to show the effect of cooling rate on phase transformations. Reproduced with permission from Cottam *et al.*, Metals **9**, 60, 2019. Copyright 2019 MDPI; licensed under a Creative Commons Attribution (CC BY) license.

additive manufacturing.[55] In alloy design, various frameworks have been proposed utilizing data-driven models such as Bayesian Network Classifiers (BNCs) to investigate the extensive design space of alloy compositions (determining viable element ranges) and Gaussian Process Regression (GPR) to optimize specific mechanical properties (e.g., strength, ductility) as a function of composition.[55] The principal insight for alloy design is the focus on constructing surrogate models derived from high-fidelity simulations or experiments, iteratively enhancing data sets through techniques such as Markov Chain Monte Carlo (MCMC) and employing these models for rapid exploration and exploitation of the compositional design space, especially for intricate, multi-objective tasks.[55]

Kouraytem *et al.*[56] presented an extensive analysis of data-driven methodologies for alloy design in the realm of metal AM, highlighting the ways in which these techniques enhance conventional physics-based models. Data-driven alloy design employs machine learning, statistical modeling, and data mining to investigate composition–processing–structure–property correlations without the necessity of explicit physical equations. Methods

include Gaussian process regression, artificial neural networks, genetic algorithms, and deep learning are emphasized for purposes such as optimizing alloy compositions, predicting mechanical performance, and delineating process–property relationships.[56] They suggested that incorporating outputs from physics-based simulations (e.g., CALPHAD, phase-field, DFT) into data-driven models will facilitate the swift prediction and optimization of alloy compositions with specific properties, thereby promoting a data-driven strategy to expedite alloy design and qualification in additive manufacturing.[56]

Historically, the process–structure–property (PSP) paradigm has maintained its foundational concepts since the emergence of materials science and engineering in the advancement of materials.[57] This paradigm shows the link among processing methods, microstructure, and the performance of the materials that can be employed for various applications with the desired properties for a specific demand.[58] However, modern materials systems are getting more complex, and application-specific performance and sustainability practices are in more demand. Consequently, one needs a more all-encompassing and comprehensive framework. This demands modification from the conventional PSP paradigm. The limits of the PSP technique are highlighted by aspects including the origin and features of the feedstock as well as the necessary performance criteria in practical applications. A more all-encompassing approach that can allow several processing constraints and design freedoms given by advanced manufacturing techniques, including AM, is much sought after. Addressing these challenges necessitates a novel paradigm. The development and design of materials can be accomplished holistically using the cycle of feedstock, processing, structure, property, and performance (FPSP^2) as shown in Fig. 3. Together with its intended use, the features of the feedstock, the material's performance in that context, and the processing, structure, and properties of a material are covered within this approach. From resource extraction to end-of-life, the FPSP^2 method offers a holistic perspective of a material's lifecycle. Among the several benefits of the FPSP^2 approach are faster materials discovery, improved materials design, and enhanced sustainability.[59,60] The FPSP^2 method considers the performance requirements of specific applications as well as the environmental impact of materials to create high-performance, environmentally friendly materials.[61] Changing from the PSP to the FPSP^2 paradigm

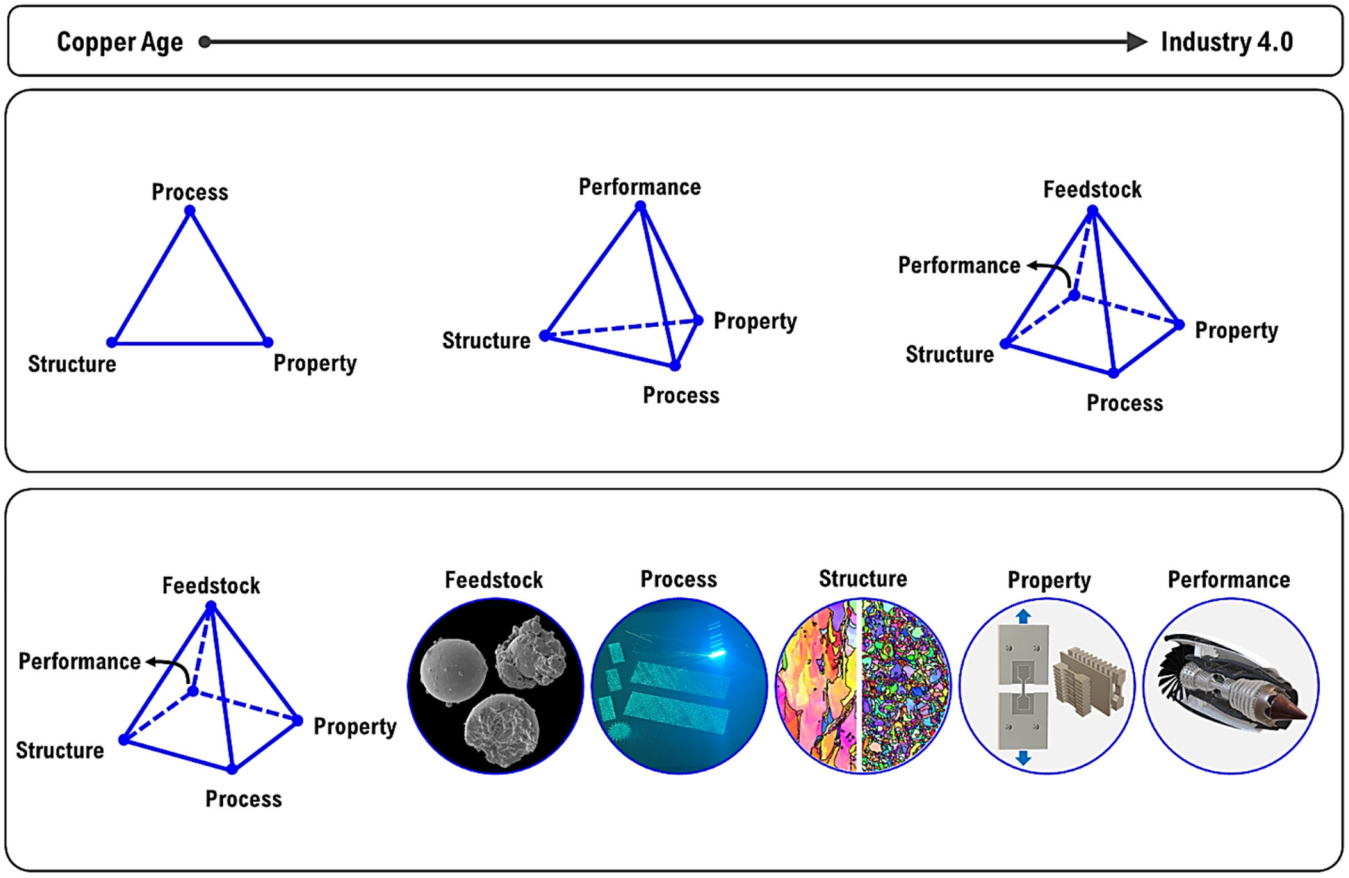

FIG. 3. Trajectory of materials science: From the copper age to Industry 4.0. From process–structure–property (PSP) to feedstock–process–structure–property–performance (FPSP^2).

may allow materials research, specifically in the context of AM, to advance significantly. By highlighting the need to assess the lifetime of all materials, this innovative method helps us to create sustainable and highly performing materials. Hence, materials scientists could open the path for development using the FPSP^2 paradigm, guiding a technologically advanced and ecologically sustainable future.

IV. UNDERLYING MECHANISMS IN GRAIN STRUCTURE CONTROL OF AM Ti ALLOYS

Although metal AM provides unparalleled design freedom, the rapid heating and cooling cycles, arising from AM's nature, can result in quite different microstructures compared to the conventionally processed alloys.[62,63] Understanding these microstructures is essential because of their direct influence on the mechanical properties of AMed components. One unique feature of metal AM components is the development of a columnar grain structure marked by elongated grains that preferentially extend along the build direction.[64,65] The main reasons for developing such a columnar grain structure are epitaxial grain growth and directed heat transfer during the AM process. A thermal gradient develops when layers build one on top of one another during printing. Upon melt pool formation, heat quickly moves to the previously deposited layers and substrate.[66,67] Moving essentially parallel to the material deposition direction, this directed heat transfer promotes grain growth in line with a temperature gradient, causing solidification in a particular crystallographic direction. By implementing *in situ* thermal measurement tools, the temperature gradient produced during layer-by-layer deposition of additive manufacturing process can be recorded.[68] Direct heat transfer usually follows the build-up direction and helps both grain formation in line with the temperature gradient and directional solidification.[69,70] Usually nucleating and expanding onto its grains, each next layer solidifies and adopts the orientation of the layer below it. Epitaxial development generates the characteristic columnar structure by spreading the grains across several layers and lowers the interfacial energy between the deposition metal and the pre-existing solid phase, which is shown in Fig. 4. Usually, the preferred direction of growth during solidification in cubic metals is the ⟨100⟩ crystallographic orientation.[69,71] The unequal surface area of the material may cause its mechanical characteristics, such as ductility and strength, to be anisotropic. Parts printed by AM will exhibit anisotropic mechanical properties if their grain structure is columnar. This may render them undesirable for engineering components that necessitate uniform mechanical properties in different directions.[72] Furthermore, fatigue resistance could be lowered since cracks might form and spread along the columnar grain boundaries. Thus, managing the grain structure by means of process parameters, inoculation procedures, substrate heating, or post-processing thermal treatments is important to attain the intended mechanical properties in metal AM components for various applications.

A. Model for analytical microstructural development

1. Model of dendrite growth by Kurz, Giovanola, and Trivedi (KGT)

Dendritic solidification greatly affects the ultimate microstructure and, thus, the properties of metal alloys. In many solidification techniques, achieving the intended microstructures requires understanding dendritic growth and nucleation. Often referred to as Ivantsov Marginal Stability (IMS), the Kurz–Giovanola–Trivedi (KGT) model[74] links alloy composition, thermophysical properties, and processing conditions to significant parameters such as the dendrite tip radius and growth velocity, providing an analytical framework for predicting dendrite growth kinetics.[75,76] Transformed from its governing equations, the KGT model depends on many simplifying presumptions like liquidus slopes, constant solute diffusivities, and partition coefficients. Under specific circumstances, these presumptions offer an analytical solution explaining the relationship between dendritic tip radius and velocity. The model is a helpful tool for estimating the features of the resulting product, even if it does not fully depict the complicated solidification process.[75] The model supposes low stability of a dendritic tip. The correct assessment of factors like liquidus slopes and partition coefficients determines the prediction efficiency of the KGT model. Collecting parameters for multi-component alloys requires the CALculation of PHAse Diagrams (CALPHAD), therefore enhancing the precision and relevance of the model to practical alloy systems.[77–79] CALPHAD data integration enhances the KGT model to produce more consistent estimations of dendritic growth behavior in complex alloy compositions.[80] The KGT model predicts microstructure evolution in numerous solidification processes, including AM, casting, and welding.[81–83] One must understand that the model's limitations are inherently defined by its simplicity. Advanced models, such as phase-field simulations, increase simulation complexity even if they provide a more thorough approach. Still, especially with analytical models, the KGT model is necessary for comprehending dendritic growth dynamics and how it influences microstructure evolution.[74] Analytically solving the formulas will let one find the influence of alloy composition on dendritic development kinetics.

2. Novel model for grain nucleation

Control of the microstructure and improvement of the mechanical properties of metallic materials depend on grain texture and grain refinement.[84,85] The transition from columnar to equiaxed grains result in substantial changes in alloy properties, including strength, ductility, and fatigue resistance. Prediction and control of resultant grain structure in solidification systems depends on the exact modeling of grain nucleation. An analytical way for estimating new grain nucleation during solidification is provided by the Gäumann adjustment of Hunt's columnar to the equiaxed transition (CET) model.[86,87] This idea holds that all nucleation sites immediately activate after undercooling to a critical threshold (ΔT_{nuc}). This clearly offers a reasonable method for calculating grain size depending on pertinent factors such as dendritic growth rates, undercooling, and nucleation site density. The Gäumann-modified Hunt CET model depends critically on the nucleation site density (N_0), which represents the total number of potential nucleation sites per unit volume.[88–90] This statistic must be calibrated using experimental data, such as grain size measurements. Moreover, experiments involving inoculated particles help to influence and enable the adjustment of this parameter. Perfect adjustment of N_0 and complete awareness of the link between grain

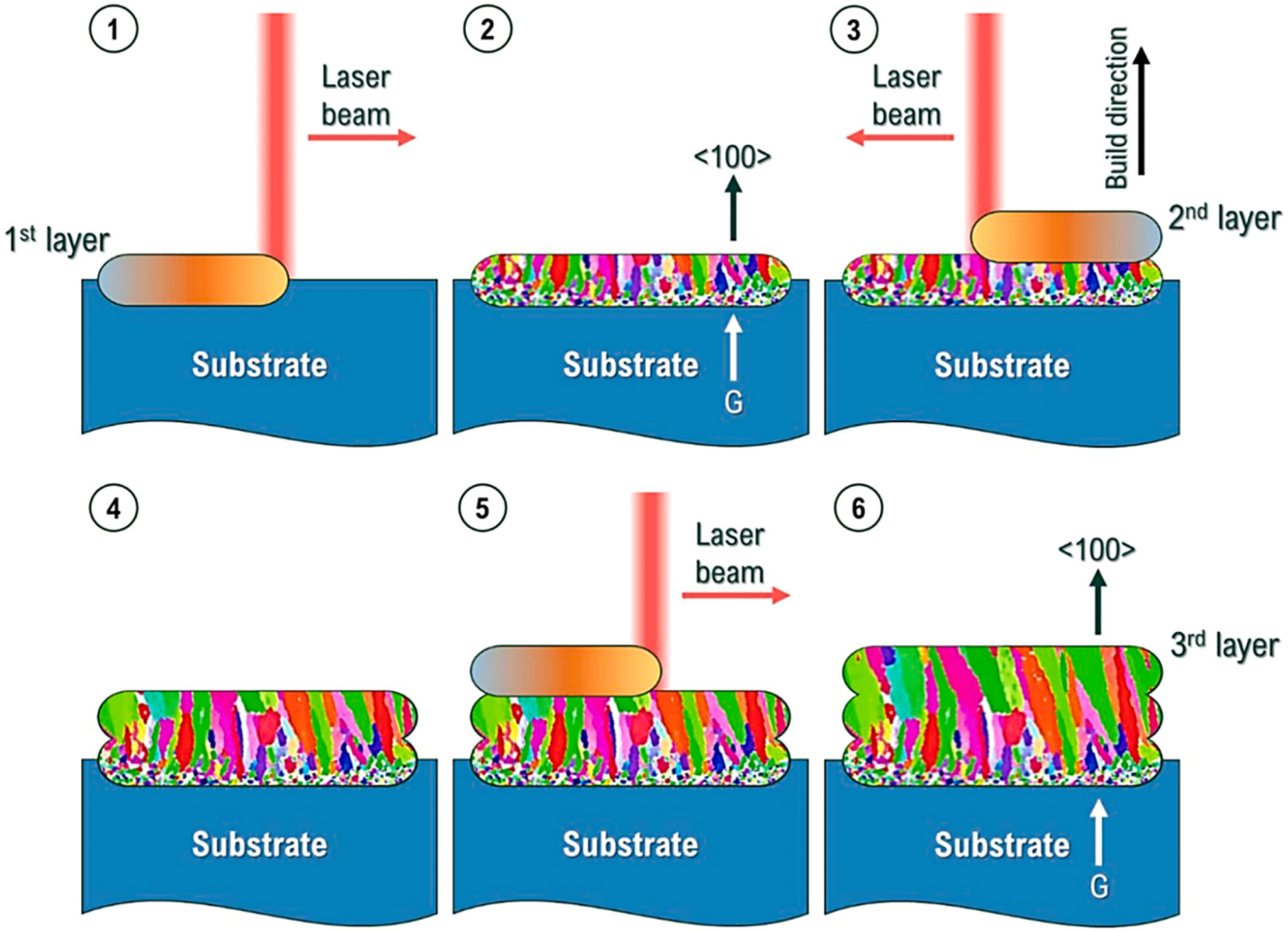

FIG. 4. Grain structure evolution in metal additive manufacturing: schematic representation of directed energy deposition (DED) process. ① and ②: most of the grains for the cubic metals will grow along ⟨100⟩ since the first layer is deposited onto the substrate and the thermal gradient direction is parallel to the build direction. ③ and ④: the second layer is deposited over the first layer; due to epitaxial development, the grains in the second layer often follow the growth direction of the pre-existing layer in the first layer. ⑤: the third layer is deposited on top of the second layer; ⑥: again, due to the thermal gradient direction parallel to the building direction, the epitaxial growth will expand and produce a columnar microstructure spanning the building direction.[73] Reproduced with permission from Alipour *et al.*, Mater. Sci. Eng. A. **921**, 147593 (2025).[73] Copyright 2025 Elsevier.

structure and processing parameters determine the correctness of the model. Often derived from the KGT model, the Gäumann-modified Hunt CET model evaluates the degree of grain nucleation and related grain refining using dendritic growth kinetics data.[91,92] By matching dendritic development characteristics with nucleation parameters, the model describes microstructure development during solidification. The model is a valuable tool for anticipating and managing grain structure in the solidification of casting, welding, and AM notwithstanding its constraints resulting from simplifying assumptions and the necessity for experimental calibration. The CET model was modified by Gäumann according to the findings of the original Hunt CET model.[93] It is hypothesized that all nucleation sites activate at the undercooling ΔT of the liquid ΔT_{nuc}. Since the density of nucleation sites (N_0) cannot be physically measured, it must be calibrated depending on experimental data (e.g., granule size). N_0 can be controlled in experiments using inoculant particles.[93]

3. Findings from novel model for grain nucleation

Especially in the field of AM, the new grain nucleation model offers major novel approaches to the control of grain structure during solidification processes.[51,94–96] Understanding these ideas is crucial since the mechanical characteristics of a material, such as strength, ductility, and fatigue resistance, depend much on its grain structure. The model offers a framework for changing the

microstructure to meet specific performance criteria by examining relationships among dendritic formation, nucleation, and processing components. The model helps to define dendritic consistent-state development. Dendrites preserve a regular form as they develop during solidification. This dynamic mechanism allows steady-state development through species' diffusion at the dendrite tip.[97] Developing basic models needed for alloy design depends on understanding the development of dendritic geometry, as shown in Figs. 5(a) and 5(b). Figure 5(a) illustrates the steady-state growth of a dendrite tip while simultaneously preserving its morphology,

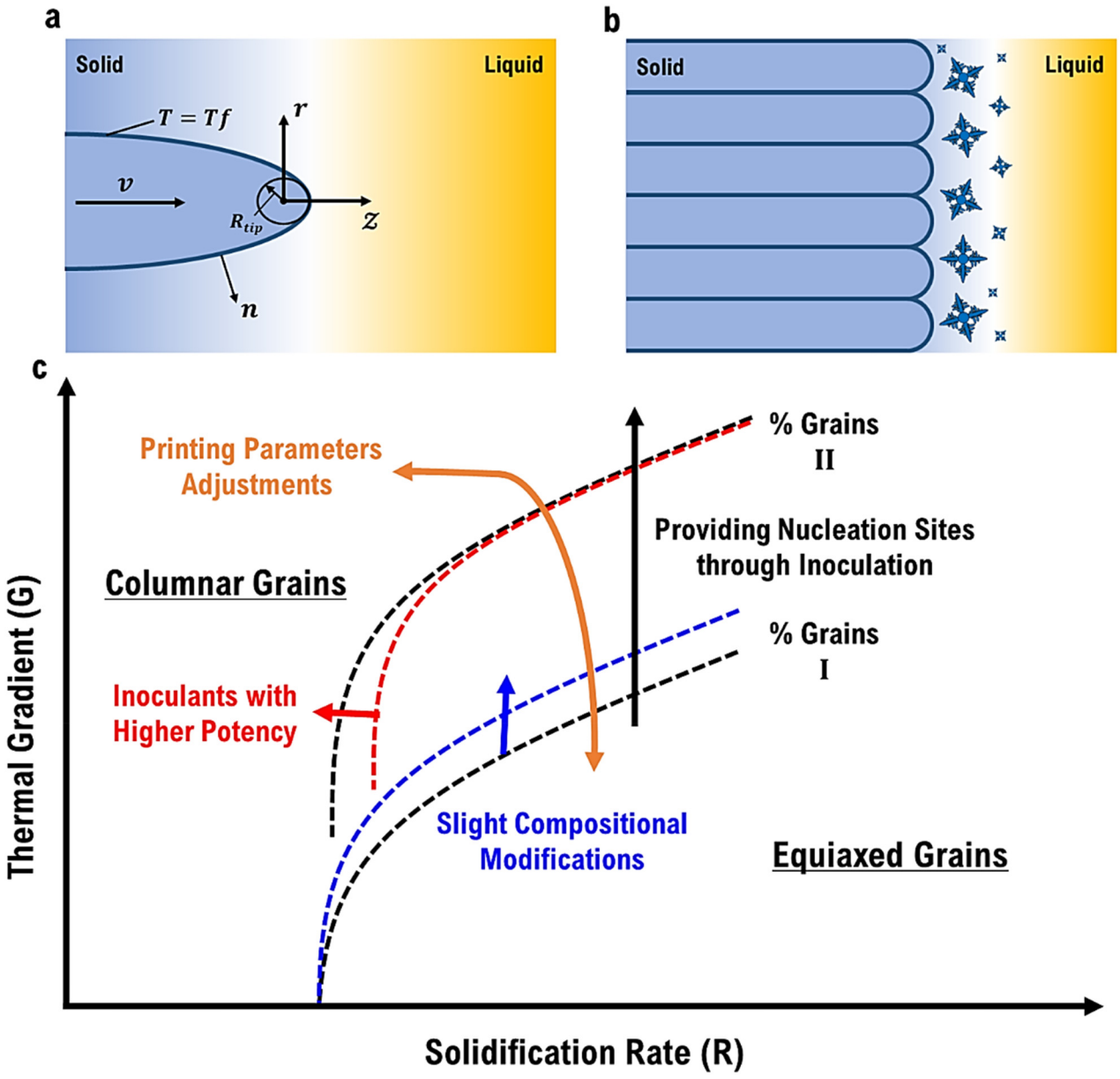

FIG. 5. (a) Steady-state growth of a dendrite tip while maintaining its shape, where *V* is the normal speed needed to keep the shape of the steady state and n is the speed at which the dendrite tip grows, (b) a schematic depicting columnar grains on the left developing along the horizontal temperature gradient, and equiaxed grains originating from nucleation sites in the liquid on the right, (c) the thermal gradient (G) vs solidification rate (R) diagram as a tool for grain structure control of solidified metals and alloys. The schematic diagram illustrates the effect of minor adjustments to composition, potent inoculants, varying AM processing parameters, and the addition of nucleation sites on the grain refinement of an additively manufactured alloy.

where V is the normal speed required to maintain the shape of the steady state and n is the rate at which the dendrite tip develops. Figure 5(b) also shows the development of columnar grains along the horizontal temperature gradient on the left and equiaxed grains that originate from nucleation sites in the liquid on the right. The grain structure is significantly influenced by the CET, and the new grain nucleation model elucidates the mechanisms that drive this transformation. The equilibrium between the nucleation and development of equiaxed grains in the undercooled liquid before the solidification front and the formation of columnar dendrites from the substrate defines the CET.[89] Changing the alloy composition or processing parameters can help to enable either columnar or equiaxed grain growth. A convincing way to show the factors influencing grain shape is provided by the temperature gradient (G) against the solidification rate (R) in Fig. 5(c). This figure shows how several factors can change the boundary between regions where columnar and equiaxed grains are preferred. For example, introducing effective inoculants improves the nucleation rate and promotes equiaxed development, hence pushing the curve to the up. In addition, the slight compositional modifications, inoculants with higher potency, and adjusting printing parameters can shift the G–R curves positions to expand or limit the equiaxed/columnar regions. Theoretically, the new grain nucleation model provides a means of understanding how different factors affect the G vs R diagram and, hence, the resulting grain structure.[98–101] The model development enables the prediction of the effect of changes in processing parameters or alloy composition on dendritic growth and nucleation, hence optimizing solidification processes to achieve the desired grain structures. This is especially relevant for AM since different temperature conditions usually produce complex microstructures. Attaining suitable mechanical properties in AM depends on the control of grain structures. To enable equiaxed grain formation, enhance homogeneity, and improve ductility, the new grain nucleation model may expand the processing parameters window, including laser power, scan speed, and layer thickness.[102–105]

V. NOVEL PROPOSED APPROACHES FOR MICROSTRUCTURAL AND MECHANICAL DEVELOPMENT

Zhang *et al.*[106] addressed the issue of obtaining fine-grained microstructures in laser powder bed fusion (LPBF) Ti alloys, which generally display unfavorable columnar grains resulting from rapid solidification and elevated temperature gradients. To address this roadblock, the authors provide a novel method utilizing titanium–copper (Ti–Cu) alloys, emphasizing copper's significant constitutional supercooling potential as a grain refiner. Unlike other widely used engineering alloys, titanium lacks commercially available grain refiners, which makes this approach somewhat unique. Presenting a feasible grain refining technique, the study shows that the selective addition of copper helps the attainment of a fully equiaxed, fine-grained microstructure in as-printed Ti–Cu alloys without requiring specialized process controls or post-processing treatments. In this approach, copper solute accumulates at the solid–liquid interface, as shown in Fig. 6(c), which increases the supercooling zone (ΔT_{cs}) and facilitates heterogeneous nucleation, generating fine, equiaxed grains. By contrast, Ti-6Al-4V shows little constitutional supercooling, producing coarse columnar grains [Fig. 6(a)]. Figure 6(d) quantitatively supports this by showing that, in comparison to traditional AM titanium alloys, Ti–Cu alloys achieve around 100% equiaxed grains with grain sizes of 10 μm. Furthermore, the intrinsic heat cycles during the AM process contribute to producing an ultrafine eutectoid microstructure ($\beta \rightarrow \alpha + Ti_2Cu$). Figures 6(e) and 6(f) demonstrate that although the initial layer develops martensite due to cooling, the thermal cycling of succeeding layers generates a refined eutectoid lamellar structure. The schematic cooling cycle design [Fig. 6(g)] reveals how the cooling rate affects phase transformation.

As Fig. 6(h) shows, transmission electron microscopy (TEM) supports the presence of an ultrafine eutectoid lamellar structure in the Ti–Cu alloys. With copper-rich areas orienting with Ti_2Cu lamellae and hyper-eutectoid particles, high-angle annular dark-field (HAADF) imaging and x-ray energy dispersive spectroscopy (XEDS) mapping clarify the distribution of titanium and copper [Figs. 6(i)–6(k)]. Further supporting the eutectoid composition of the lamellar structure is the presence of about 2.8 wt.% Cu in α-Ti and 39.1 wt.% Cu in Ti_2Cu. Zhang *et al.*[106] clarified the nanoscale features enhancing the mechanical properties of the Ti–Cu alloy. The mechanical properties of the as-printed Ti–Cu alloys show a unique combination of yield strength and ductility compared to conventionally manufactured Ti alloys. The fracture analysis validated the tensile test results [Figs. 6(n)–6(p)], which shows that while the Ti–8.5Cu alloy displayed a brittle fracture surface, the Ti–3.5Cu alloy displayed ductile fracture behavior. The results show that changing the copper amount in the Ti–Cu alloy results in different mechanical properties. The authors suggest that this alloy design could be expanded to other eutectoid alloy systems, therefore enabling improved microstructure control and performance of AM components for biomedical and aerospace applications.

Song *et al.*[107] addressed the challenge of designing strong and ductile titanium alloys using intentional oxygen and iron inclusion, two common and useful alloying elements typically difficult to combine. Combining alloy design with direct energy deposition (DED) AM helps the authors address the problems of oxygen-induced embrittlement and iron's microsegregation tendencies. Using off-grade sponge titanium or waste materials reduces the carbon footprint connected with conventional titanium production, and the development of a new category of titanium–oxygen–iron (Ti–O–Fe) alloys displays outstanding tensile characteristics. The result of this manufacturing process is shown in the form of finished rectangular coupons [Fig. 7(a)]. Careful microstructural control produces fine equiaxed prior-β grains and a refined α-β lamellar architecture, hence explaining the improved properties of the AM-processed Ti–O–Fe alloys. DED process simulations helped to create a processing window promoting the α–β transformation while maintaining high cooling rates [Figs. 7(b) and 7(c)]. The EBSD and SEM images show the improved structure brought about by oxygen addition [Figs. 7(d)–7(k)]. The microstructural characteristics, along with the distinctive partitioning behavior of oxygen and iron, increase the alloy's mechanical properties. iDPC-STEM imaging [Figs. 7(m) and 7(n)] specifically confirms the segregation of oxygen to the α-phase rims adjacent to α/β contacts, resulting in nano-heterogeneity characterized by ductile

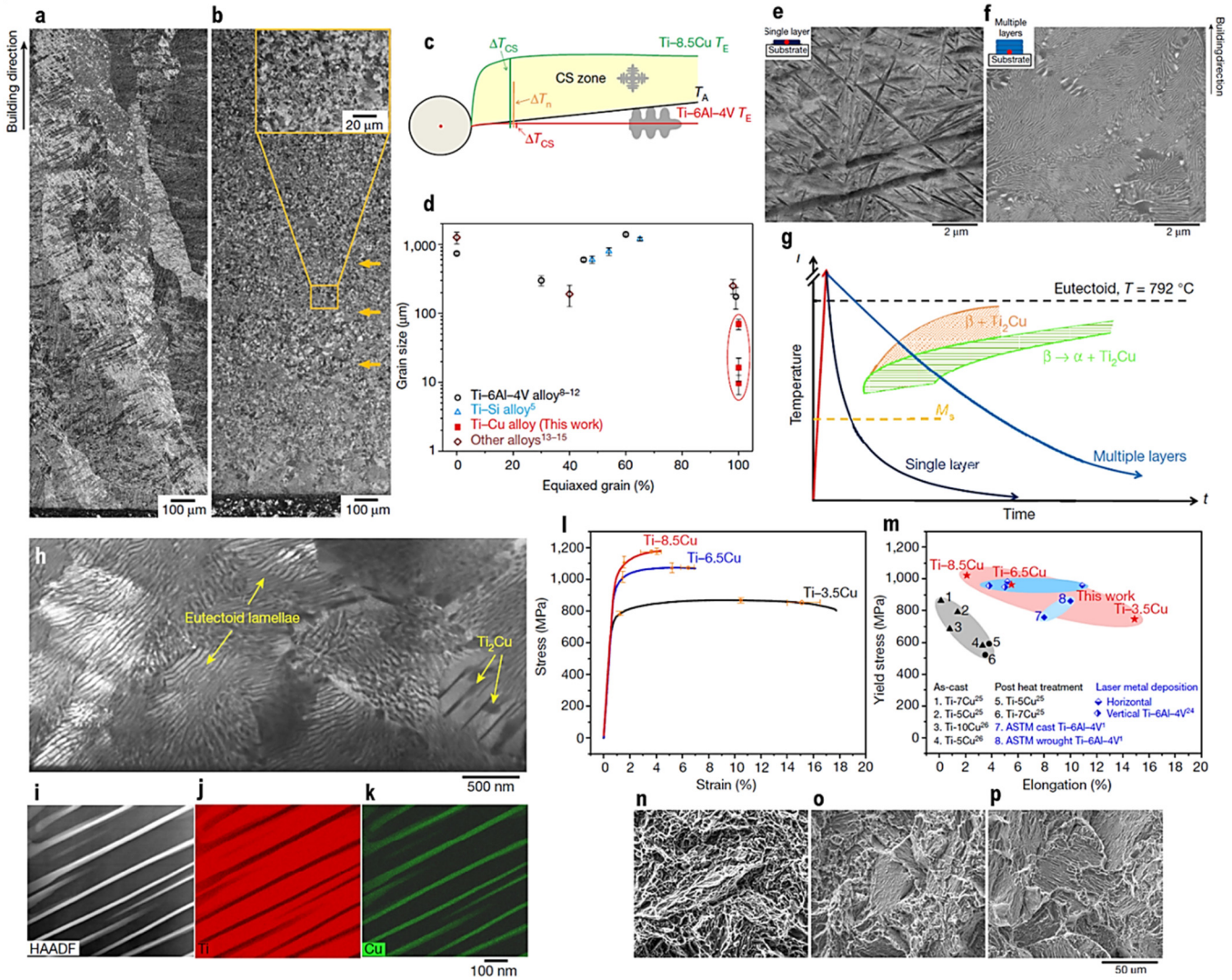

FIG. 6. LPBF of Ti–Cu to produce an ultrafine-grained with the high-strength Ti alloy. (a) and (b) Optical micrographs of Ti-6Al-4V and Ti—8.5Cu alloys as-printed, respectively. (c) Schematic diagram of the grain growth mechanism of Ti—8.5Cu and Ti-6Al-4V alloys, (d) summary of the area percentage of equiaxed grains vs grain size for the as-printed titanium alloys. (e) and (f) The microstructure evolution at the first layer (represented by the red patches) of the as-printed Ti—8.5Cu alloy is shown in SEM-BSE images during the AM process. (g) A schematic continuous cooling transformation diagram illustrates various solid-solid phase transformation pathways for the laser deposition of the first and subsequent layers. (h)–(k) The elemental profiles for Ti and Cu and the TEM characterization of the as-printed Ti—8.5Cu alloy are provided. (n)–(p) Tensile properties of as-printed Ti–Cu alloys and the yield strength vs tensile elongation to failure for Ti–Cu alloys manufactured by different methods and required values by ASTM standard, (l) and (m) SEM-BSE for fractography of the Ti—6.5Cu and Ti—8.5Cu alloys. Reproduced with permission from Zhang *et al.*, Nature **576**, 7785 (2019).[106] Copyright 2019 Nature.

interiors and robust edges. These elements contributed to higher strength and ductility than the traditionally cast Ti–Fe alloys.

Essential new perspectives on the strengthening mechanisms of these alloys can be explained through atomic-scale characterization. The higher concentration of oxygen at the periphery of the α-phase adjacent to the α/β interfaces is quantitatively supported by atom probe tomography (APT) data [Fig. 7(o)], which corresponds with the increase in bonding attributed to the strengthened local electric field in the vicinity, resulting from the marked electronegativity of oxygen atoms [Figs. 7(p) and 7(q)]. Furthermore, the HAADF-STEM imaging [Fig. 7(r)] displays an uneven distribution of Fe in the β-phase, hence generating localized strain fields that prevent dislocation migration. The oxygen lattice in a high oxygen content alloy limits dislocation motion by preventing additional dislocation propagation. Hence, coordinated effects of oxygen and iron partitioning define enhanced mechanical performance of the

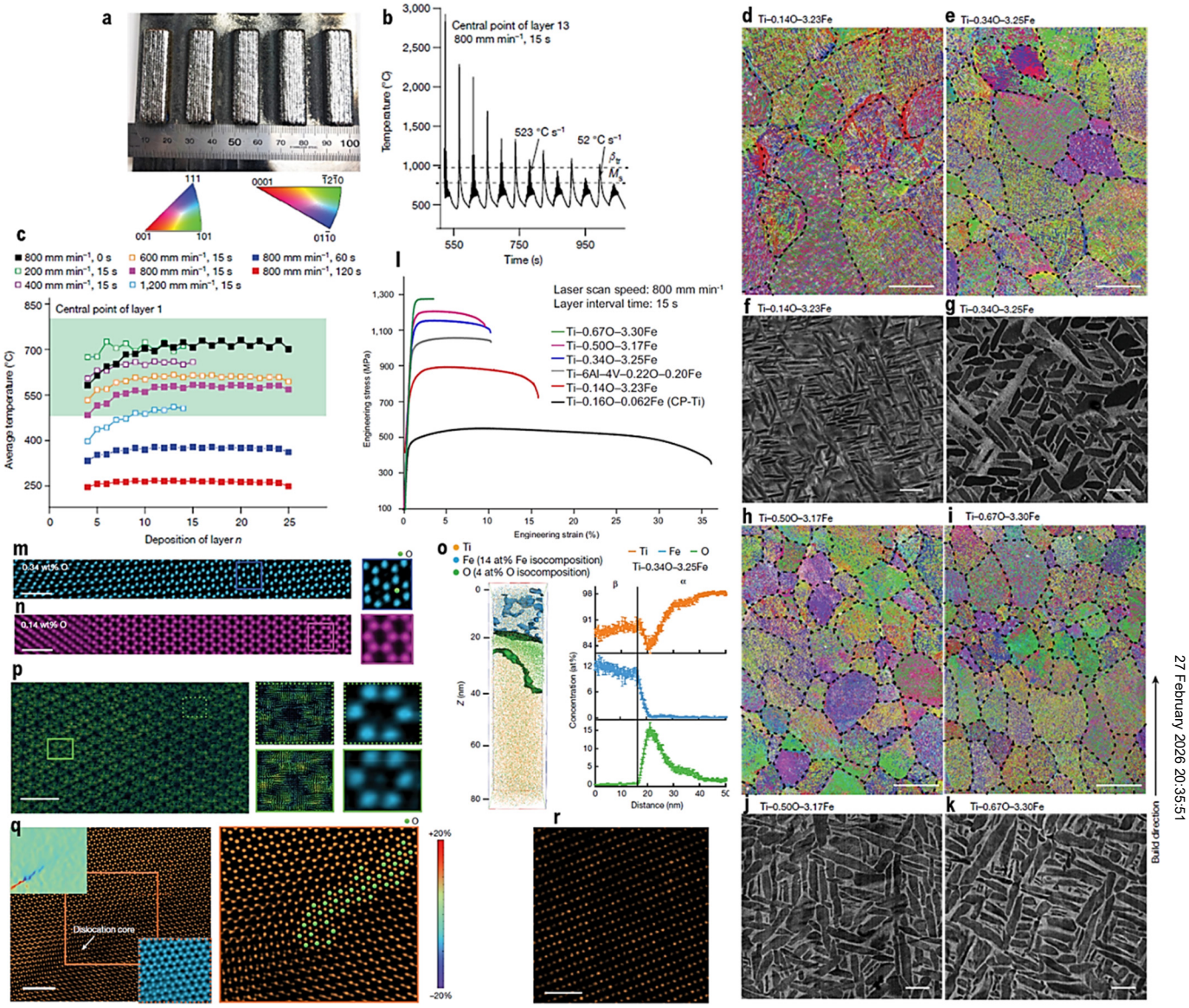

FIG. 7. Strong and ductile titanium–oxygen–iron (Ti–O–Fe) alloys produced by the DED process. (a) As-built rectangular 3D-printed Ti—0.34O—3.25Fe coupons, (b) and (c) temperature profile of the central point of layer 13 in a 25-layer coupon generated by simulation, along with the processing window (green zone) determined by simulation. (d)–(k) EBSD and SEM-BSE images of the printed Ti—0.14O—3.23Fe, Ti—0.34O—3.25Fe, Ti—0.50O—3.17Fe, and Ti—0.67O—3.30Fe alloys, (l) tensile properties of DED-printed Ti–O–Fe alloys at room temperature, (m) and (n) iDPC-STEM images of the α/β interfaces in Ti—0.34O—3.25Fe and Ti—0.14O—3.23Fe alloys, (o) APT data from Ti—0.34O—3.25Fe, illustrating the O atoms' propensity to segregate toward the α-phase margins near the α/β interfaces. (p) Tensor flow, (q) HAADF-STEM image of a dislocation inhibited by an O interstitial array, (r) a HAADF-STEM image of a β-phase region, highlighting the non-uniform distribution of Fe, shown by the uneven Z-contrast, for which the zone axis is [110]β, and DPC-STEM images along a [0001]α direction. Reproduced with permission from Song *et al.*, Nature **618**, 7963 (2023). Copyright 2023 Nature; licensed under a Creative Commons Attribution (CC BY) license.

alloy. Unlike other Ti alloys, DED-printed Ti–O–Fe alloys exhibit a well-balanced mix of ultimate tensile strength and total elongation. Studies of the tensile fracture surface and HAADF-STEM pictures of dislocations [Figs. 7(p)–7(r)] support this. The Ti–O–Fe alloys' higher volume percentage of oxygen-free β phase helps to induce deformation, hence improving the balance of tensile properties. This work shows the possibilities of off-grade sponge titanium as a feedstock and the production of high-performance titanium–oxygen–iron alloys by carefully modifying alloy chemistry and AM process parameters. The knowledge gained helps future interstitial

engineering methods to reduce embrittlement in Ti alloys to be developed to widen the use range of this advanced material.

Zhu *et al.*[108] proposed a novel approach in developing AMed Ti alloy with exceptional mechanical properties. They produced a commercial β-titanium alloy (Beta-C) using LPBF and, with a simple post-heat treatment, obtained a tensile strength above 1600 MPa while keeping favorable elongation. The considerable improvement is ascribed to the formation of unique, dense, stable, and internally twinned nanoprecipitates, which are infrequently encountered in traditionally processed Ti alloys, providing a feasible path for manufacturing high-performance structural Ti materials. Particularly, the ultimate tensile strength (UTS), obtained after heat treatment, Fig. 8(a) shows the outstanding mechanical properties enhancement. In addition, these findings are displayed together with pertinent materials in Fig. 8(b). Unlike conventional Ti alloy processing techniques, Zhu *et al.*[108] demonstrated that the as-built LPBF microstructure, distinguished by a high density of dislocations mostly of screw character, is an essential precursor for the subsequent development of nanotwinned α-precipitates during post-heat treatment, confirmed by XRD analysis in Fig. 8(d). Molecular dynamics simulations [Figs. 8(l)–8(p)] clarify this phenomenon, indicating that these dislocations reduce the energy barrier for α-precipitate nucleation and facilitate the development of numerous twin variations in close proximity. Additionally, HAADF STEM imaging demonstrates the lack of grain boundary α, diverging from traditionally produced alloys, resulting in a more uniform microstructure with enhanced mechanical stability.

The Beta-C Ti alloy is characterized by internally nanotwinned α-precipitates [Figs. 8(f)–8(h)], exhibiting an average twin thickness of 7.5 nm. Atomic-scale HAADF-STEM imaging verifies the existence of {1011} twin borders, together with the rarer basal-pyramidal and {1013} twins at the terminus of the twins, hence augmenting the structural complexity and stability of the precipitates. The precipitates conform to the Burgers orientation relationship with the β-matrix [Fig. 8(j)], which is essential for the coherent growth and stability of the precipitates. The atomic-resolution HAADF-STEM image in Fig. 8(i) illustrates that the {1011} twin boundaries are locations of periodic solute segregation, characterized by the accumulation of Mo/Zr atoms. The as-built dislocation structure's synergistic interaction with the growth of nanotwinned precipitates produces the amazing mechanical properties of the LPBF Beta-C alloy. Through controlled post-AM heat treatment, strength and ductility may be customized, preventing destructive grain boundary precipitates and producing a more homogeneous microstructure [Fig. 8(e)]. The MD simulation of twin variants reveals three primary forms of twin faults, more especially, the a-precipitate variants. Therefore, Zhu *et al.*[108] presented a novel method for fabricating high-performance Ti alloys via additive manufacturing, replacing traditional techniques reliant on precipitation in the bulk and along grain boundaries, thus paving the way for future alloy innovations and enhancing properties for critical-performance applications.

Zhang *et al.*[109] addressed the fundamental hurdles of spatial phase and physical heterogeneity in AM titanium alloys through alloy design/modification. This important challenge could jeopardize the reliability of components for real engineering applications. Through *in situ* alloying of Ti–6Al–4V using commercially pure titanium (CP-Ti) grains and iron oxide (Fe_2O_3) nanoparticles, which is coupled into a synergistic alloy design process, they attempted to overcome phase and texture heterogeneities. By lowering the concentration of vanadium (V) and including iron (Fe), this approach essentially lowers phase heterogeneity compared to the traditional workhorse Ti-6Al-4V in the Ti alloy family. This approach produced consistently spaced microstructures with enhanced mechanical properties and oxygen solute strengthening [Fig. 9(d)]. The technique highlights how alloy design can surmount obstacles in additive manufacturing through its unique design advantages. A key aspect of their approach is the uniform application of Fe_2O_3 nanoparticles onto titanium powder surfaces via a layer-by-layer surface engineering process, which is illustrated in Fig. 9(f). This controlled powder preparation method reduces the uneven mixing seen in conventional mechanical blending/blending. Figures 9(g) and 9(h) demonstrate that modifying surface charges enables Fe_2O_3 nanoparticles to bond with Ti powders, hence facilitating enhanced elemental partitioning during solidification. Kinetic simulations indicate that Fe, with greater tracer diffusivity than V, promotes enhanced elemental partitioning, leading to homogenous lamellar (α + β) microstructures upon solidification.

The newly engineered Ti alloys demonstrate significant enhancements in the uniformity of mechanical properties, especially in tensile ductility, in both vertical and horizontal build orientations, thereby overcoming a significant restriction of traditional AM Ti alloys. Figure 9(e) illustrates that the 25Ti-0.250 alloy has exceptionally consistent mechanical behavior in both vertical and horizontal orientations. The alloy reveals an increased ductility and strength levels similar to LPBF Ti-6Al-4V. Hence, exact control of CP-Ti and Fe_2O_3 additives helps to customize strength-ductility combinations to meet specific application requirements. Experiments using APT demonstrate that the alloys have different elemental partitioning: Fe and V are concentrated in the β phase, and Al and O are concentrated in the α phase [Figs. 9(l)–9(o)]. The homogeneous (α + β) microstructures in this research promote dependable mechanical properties. Utilizing alloys with an extensive surface area facilitates further reactions and improves mechanical properties. Therefore, given that temperature cycling and related phase heterogeneity are prevalent in several materials across multiple AM technologies, this design framework could enhance other alloy systems and AM processes with the proper inoculant and appropriate decoration approach.

The important issue of coarse columnar grains and robust textures in AM titanium alloys, which often lead to mechanical property shortcomings, is investigated in the work of Nartu *et al.*,[110] proposing 3D-printed Ti alloys with alloy design perspective. The authors established a computational approach to enable the choice of alloying additives promoting a CET during AM, hence addressing this challenge. They propose and analyze two rival CET mechanisms: growth limitation by constitutional supercooling, an expanded freezing range (ΔT), and elevated cooling rates characteristic of AM. Their studies seek to provide accurate mechanistic understanding for additive manufacturing design using two concepts for CET: solidification and growth restrictions. Figures 10(a)–10(e) show the chemical compositions of titanium-based alloys, especially Ti–V and Ti–Mo, and showcase the improvement of grain

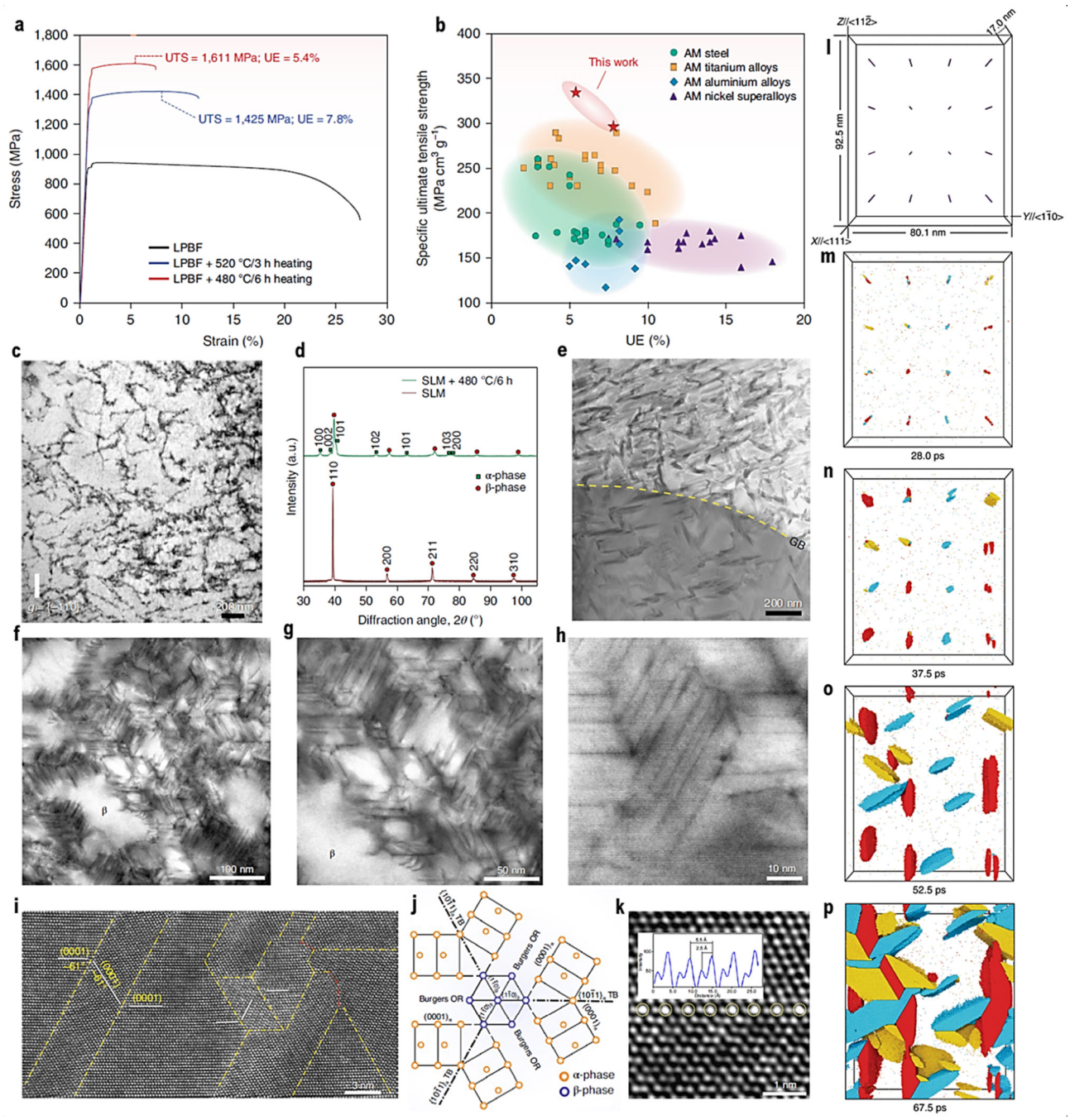

FIG. 8. Ultrastrong nanotwinned Beta-C Ti alloys through LPBF and post-heat treatments. (a) Engineering stress–strain curves for the as-built and post-heat-treated Beta-C Ti alloys at varying temperatures, (b) correlation between the specific strength and uniform elongation (UE) of LPBF Beta-C alloys with post-heat treatments and comparison with other high-strength Ti alloys. (c) BF TEM image of the LPBF in its as-built state, (d) XRD spectra that verify the phases present in the as-fabricated and heat-treated microstructures, (e) HAADF-STEM image of the post-heat-treated condition, (f)–(h) BF-STEM images demonstrating a high number density of nanotwinned lamella contrast oriented along three dimensions that is present in the α-precipitates of post heat-treated specimens. (i) at the atomic level HAADF-STEM image from a local region in a demonstrating three α-variants, (j) schematic illustrating the Burgers OR between the β-phase and α-twin variants, (k) atomic-resolution HAADF-STEM image illustrating periodic solute segregation in the α twin boundary, (l)–(p) MD simulation of nanotwinned precipitation in the vicinity of dense screw dislocations. Reproduced with permission from Zhu *et al.*, Nat. Mater. **21**, 11 (2022). Copyright 2022 Nature.[108]

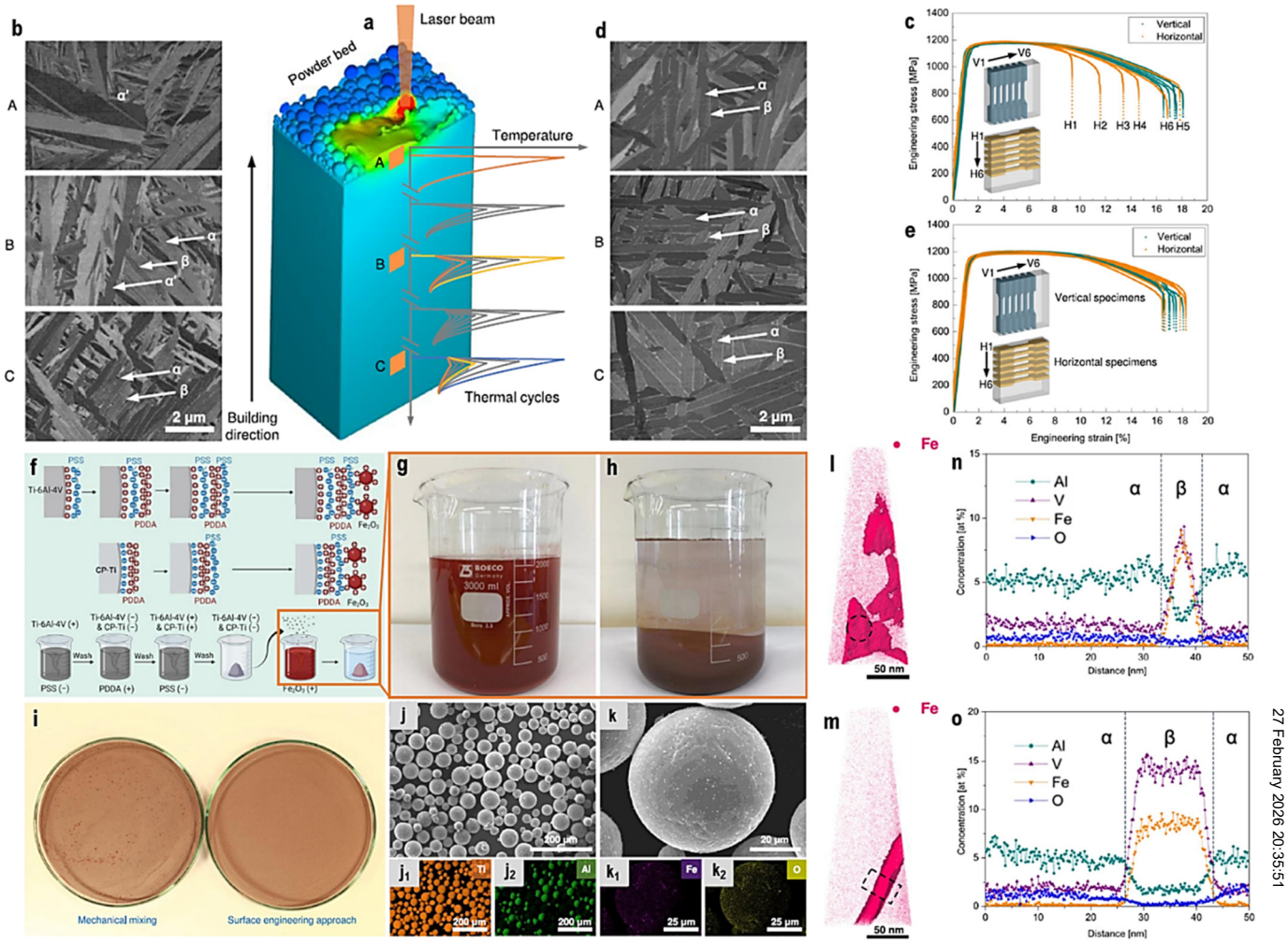

FIG. 9. Designing against phase and property heterogeneities in the newly developed 25Ti–0.25O alloy fabricated via LPBF to overcome strength-ductility trade-off. (a) The LPBF process and the intrinsic thermal cycles that different locations of the fabricated part undergo are depicted in a schematic. (b) SEM-BSE micrographs are provided to illustrate the spatially dependent phases in Ti-6Al-4V along the building direction (BD). (c) Tensile engineering stress–strain curves of Ti-6Al-4V are presented in the vertical and horizontal directions. (d) SEM-BSE micrographs illustrating the homogeneous lamellar ($\alpha + \beta$) microstructure of the recently developed 25Ti—0.25O alloy, (e) tensile engineering stress–strain curves of the 25Ti—0.25O alloy in the vertical and horizontal directions. (f) A schematic of the feedstock preparation process using the surface engineering approach, the Fe_2O_3 suspension before and after the addition of processed Ti–6Al–4V and CP-Ti particles, (g)–(i) comparison of feedstocks prepared through mechanical blending and the surface engineering method, The homogeneous distributions of both CP—Ti and Fe_2O_3 are confirmed by the SEM-BSE and SEM-EDS images (j), (k). Al, V, Fe, and O distribution is illustrated in the APT characterization of the newly developed alloys (l)–(o). Reproduced with permission from Zhang *et al.* Nat. Commun. **13**, 4660 (2022). Copyright 2022 Nature; licensed under a Creative Commons Attribution (CC BY) license.

structure control through the CET. The work of Nartu *et al.*[110] shows that insufficient growth limitation factor Q derived from increasing alloy content produced a non-ideal microstructure. In this study, the impact of the manufacturing processes of DED and LPBF on microstructural development was investigated. Figures 10(g)–10(k) clearly show that the homogeneous textures were similar, even if the heat gradients were somewhat different. Furthermore, both techniques could generate components with homogeneous strength and equiaxed grains. Therefore, using an appropriate alloy choice and a large volume of a solid solution helps to reach a high CET free from the impact of AM variables. Analyzing the solidification rate during alloy manufacture helps one to do this by means of a significant increase in ΔT before solid nucleation, hence refining the alloy composition.

Barriobero-Vila *et al.*[111] investigate the challenge of strong crystalline texture and anisotropic properties in AMed Ti alloys, especially those produced by selective laser melting. They proposed a novel inoculant to address these hurdles. Their approach revealed

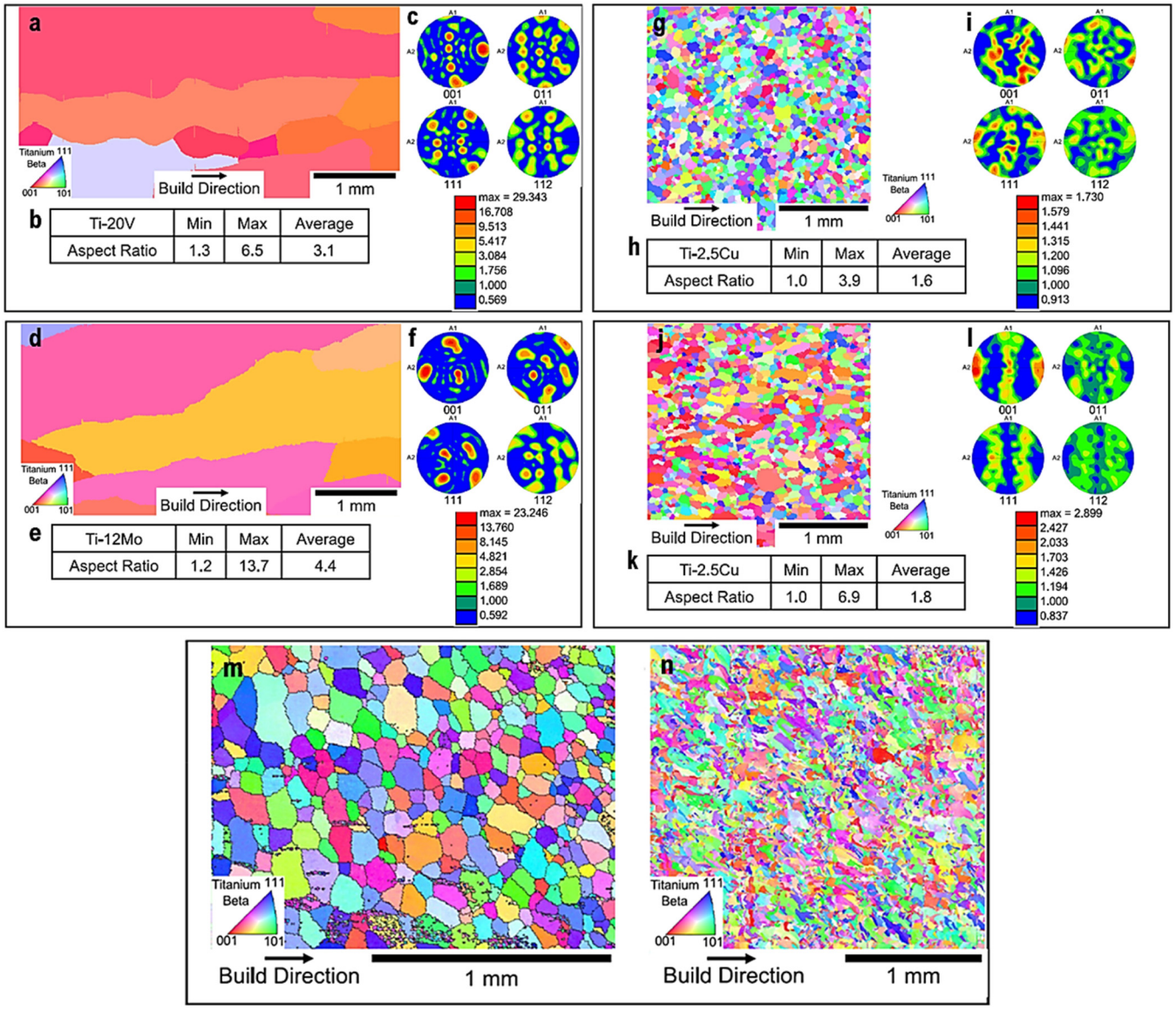

FIG. 10. Underlying factors determining grain morphologies in high-strength Ti alloys (Ti–V, Ti–Mo, Ti–Cu, Ti–Al–V–Fe) processed by LPBF and DED. EBSD-IPF, average aspect ratios of the grains, and EBSD-pole figures of (a)–(c) Ti–20V and (d)–(f) Ti–12Mo specimens showing the coarse columnar grain morphology with moderate texture in the microstructure, whereas the (g)–(i) Ti–2.5Cu and (j)–(l) Ti–6.8Cu specimens exhibited the refined grains with the equiaxed morphology as well as a weak texture. Comparison of microstructures of alloys processed using DED and LPBF processes, (m) DED Ti-185 alloy and (n) LPBF Ti64 + 5Fe alloy highlighting resultant equiaxed microstructures in their as-built microstructures. Reproduced with permission from Nartu *et al.*, Nat. Commun. **14**, 3288 (2023).[110] Copyright 2023 Nature; licensed under a Creative Commons Attribution (CC BY) license.

a successful method to change the production of the α phase, which does not follow the orientation of the parent beta (β), by introducing the peritectic-forming element lanthanum (La) into commercially pure titanium (CP-Ti) as shown in Figs. 11(a)–11(e). This work suggests a method to obtain more equiaxed microstructures to reduce anisotropy and enhance the properties of AM-based Ti alloys. Unlike conventional martensitic microstructures in AM Ti alloys after LPBF, this approach uses a Ti—2 wt. %La alloy to produce a refined and twisted grain structure. The high-energy x-ray Synchrotron Diffraction (HEXRD) data track phase transfer and show a lower textural strength than CP-Ti, implying that heterogeneous nucleation has essentially limited phase orientation transfer [Figs. 11(g)–11(i)]. Barriobero-Vila *et al.* found the two investigated alloys offer an additional parameter: the concentrations

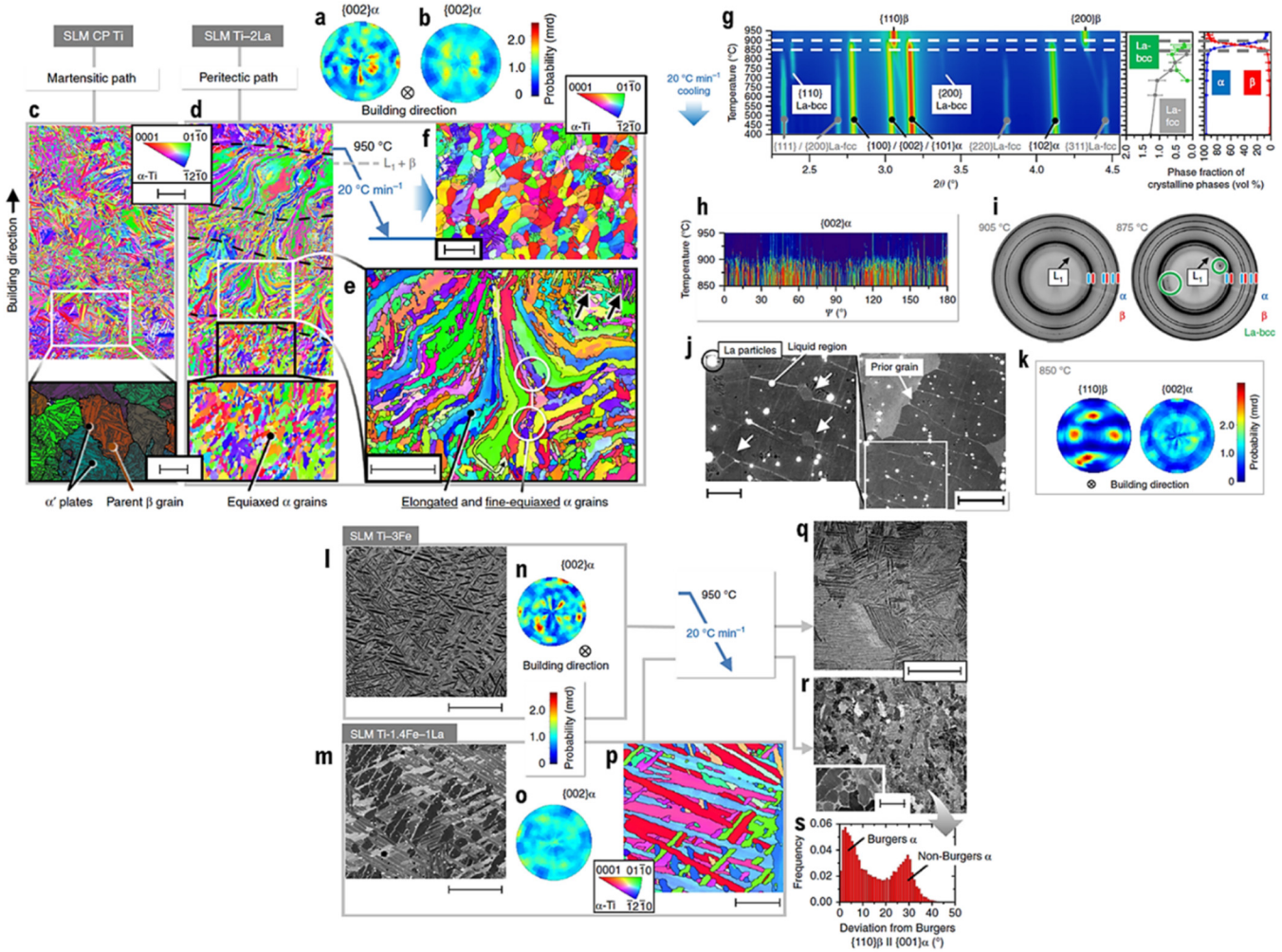

FIG. 11. Development of peritectic Ti alloys (Ti–La, Ti–Fe, Ti–Fe–La) for 3D printing. (a)–(e) EBSD-IPF and pole figures illustrating the texture alteration during LPBF of CP–Ti and Ti–2%La (wt. %). The incorporation of 2% La into CP-Ti results in a reduction of the preferential orientation of the α phase along the building direction. (f) Post-heat treatment of as-fabricated Ti–2%La through slow cooling at 20 °C min^{-1} from 950 °C, traversing the peritectic line, yields a recrystallized-like microstructure. (g)–(i) Additionally, a color-coded 2D plot illustrates the evolution of {*hkl*} reflections for β, α, La-bcc, and La-fcc at 2θ = 2.25–4.55°, alongside the concurrent evolution of volume fractions of crystalline phases derived from Rietveld analysis during continuous cooling from 950 to 400 °C at 20 °C min^{-1}, as well as normalized pole figures depicting the phase transformation kinetics of the Ti-2% La alloy. (j) The nucleation of α particles, indicated by arrows, is observable at the former β/L1 interfaces in a microstructure quenched from 950 °C. Scale bar: 5 μm (right side); 2 μm in magnified image (left side). (k) Normalized pole figures of $(110)_\beta$ and $(002)_\alpha$, reconstructed from a gauge volume of 1 × 1 × 5 mm^3, demonstrate that α does not inherit the texture of the parent β phase immediately following the β → α transformation of Ti–2La during cooling to 850 °C. The conversion of α from β (β → α) is evidenced by the swift rise in the volume fraction of α between 900 and 850 °C, as illustrated in (g). (l)–(s) It reduces solidification texture (EBSD-IPF, pole figure, and SEM-BSE) during the additive manufacturing of Ti–3Fe and Ti–1.4Fe–1La alloys in both as-built and heat-treated states, achieved through a gradual cooling from 950 °C at 20 °C min^{-1} to ambient temperature. Reproduced with permission from Barriobero-Vila *et al.* Nat. Commun. **9**, 3426 (2018).[111] Copyright 2018 Nature; licensed under a Creative Commons Attribution (CC BY) license.

that would generate unique microstructures in Ti–2.5Cu and Ti—6.8Cu alloys. Figures 11(l)–11(s) demonstrate that at 950 °C, a β-solution generates a well-aligned texture compared to the as-fabricated condition. These results show that the alloys under investigation have better mechanical characteristics; specifically, their relatively low strength and high ductility suggest potential use in AM. The alloys exhibited no orientation preference when 3D printed. They proposed that fine-tuning the composition and processing parameters will allow space to push the boundary of this approach in alloy development in the context of AM Ti alloys.

Zhang *et al.*[112] proposed a novel *in situ* alloy design process aiming at improving the mechanical properties of titanium alloys produced by LPBF. The authors present the technique to attain micrometer-scale concentration modulations (micro-CMs) to

address the constraints in AM Ti-6Al-4V alloys, particularly their sensitivity to spatial phase and microstructure heterogeneities due to intrinsic heating and cooling cycles. In the proposed approach, they mixed the Ti-6Al-4V and 316L stainless steel powders in specific ratios to optimize the unique features of every alloy component. This technique aims to produce location-specific chemical compositions within the printed components to enhance their mechanical properties, therefore opening opportunities that are difficult to attain in conventional Ti alloys and manufacturing methods. The distinctive "lava-like" microstructure, including well-defined swirls, is corroborated by SEM images [Figs. 12(d), 12(e) and 12(h)]. These swirls are created explicitly by combining titanium, aluminum, and vanadium with iron, chromium, and nickel [Fig. 12(a)]. The mixing results in regions becoming $\beta + \alpha'$, and the volume fractions can be ascertained through meticulous characterization. To achieve this fine-grained structure and subsequently produce positive outcomes akin to other techniques, such as High-Power Impulse Magnetron Sputtering (Hip-IMS), it implies that future research may provide advantages by employing comparable deposition rates.

Microstructural characterizations, such as SEM, TEM, and APT, offer substantial evidence for forming a fine-scale, modulated dual-phase ($\alpha' + \beta$) microstructure in the Ti64 + SS316L specimens. In this unique microstructure, the β phases are highly scattered throughout the α' martensite matrix, exhibiting a uniform density without directionality or clumping. Through controlled architecture, the design has achieved crucial microstructural properties, most notably a nanoscale high dislocation density with a spacing of approximately 20 nm. The Ti64-(4.5%)316L microCM alloy exhibits an exceptional combination of high yield strength (~1.3 GPa), significant uniform elongation (~9%), and superior work-hardening capacity (>300 MPa), as shown in Figs. 12(n)–12(q). These characteristics demonstrate a combination of strength and ductility surpassing that of common Ti alloys manufactured by standard manufacturing techniques. The efficacy of this *in situ* design introduces innovative approaches for the fabrication of unique, high-performance Ti alloys.

Zhang *et al.*[113] offered a bifunctional alloy design approach with a focus toward the controlled molybdenum (Mo) integration into Ti-5Al-5Mo-5V-3Cr (Ti-5553) to address the persistent challenge with anisotropic mechanical properties in AM Ti alloys. By concurrently refining grains and mitigating detrimental phase transformations, the authors circumvent the constraints of traditional AM techniques, which frequently necessitate property-degrading post-processing or deal with intrinsic performance variability. This is achieved through the strategic use of Mo nanoparticles in LPBF. Zhang *et al.*[113]'s unique approach effectively decouples the negative link between strength and ductility generally observed in additive produced Ti alloys by producing a microstructure defined by fine equiaxed grains and uniform phase distributions as illustrated in Figs. 13(a)–13(d). The effectiveness of the bifunctional Mo addition arises from a synergistic interaction of mechanisms that address the fundamental drivers of microstructural variability in LPBF. In this approach, the partially melted Mo nanoparticles serve as heterogeneous nucleation sites, impeding columnar grain development and promoting a refined equiaxed microstructure. Simultaneously, dissolved Mo stabilizes the β phase, reducing undesired isothermal ω and α phases during the fast temperature cycling characteristic of LPBF. This dual action generates a microstructure that withstands thermal-induced phase instabilities, facilitating improved work hardening via a refined microstructure.

In this work, the resultant Ti-5553 + 5Mo alloy demonstrates an enhanced amalgamation of mechanical properties relative to traditional Ti-5553 and analogous alloys produced using diverse AM procedures, irrespective of post-processing. The alloy exhibits markedly enhanced and consistent tensile strength, ductility (~9% uniform elongation), and work-hardening capacity (>300 MPa), as shown in Figs. 13(e)–13(g). With remarkable repeatability of results, comparative studies of yield strength and elongation highlight the clear superiority of the newly engineered alloy over previous AM high-strength titanium alloys, so highlighting the efficiency of the designed microCM in improving both strength and ductility in 3D-printed Ti alloys. By indicating a change from coarse columnar grains to refined equiaxed structures, Mo segregation at cell borders, and a reduction in crystallographic texture, EBSD and SEM/EDS studies help explain the mechanisms involved and improve mechanical properties. Hence, Zhang *et al.*[113] presented a comprehensive approach for alloy design in additive manufacturing, emphasizing the importance of simultaneously controlling grain structure and phase stability through strategic alloying. They have leveraged the bifunctional features of Mo in Ti-5553 to develop a directly manufacturable alloy with exceptional mechanical properties, therefore obviating the need for costly and often inadequate post-processing techniques.

In the most recent study, Brooke *et al.*[114] has introduced compositional criteria that predicts the columnar to equiaxed transitions in metal AM. The ongoing source of discussion and a long-standing challenge has been the prediction of the CET and grain refinement for AM alloys from thermodynamic databases. In general, designing alloy compositions to accomplish fully equiaxed microstructures is the primary objective, as this eliminates the mechanical anisotropy that is frequently associated with the large columnar grains in AM alloys. The growth restriction factor (Q), constitutional supercooling parameter (P), and non-equilibrium solidification range (ΔT_s) are three compositional parameters that have been evaluated in the literature across a variety of Ti alloys [Figs. 14(a)–14(c)]. Brooke *et al.*[114] experimentally verified that P is the most reliable parameter to guide the selection of alloying elements for AM alloys. This was demonstrated in Ti–Fe, Ti–Cu, Ti–Cu–Fe, and Ti–Mo alloys produced via DED technique [Figs. 14(d)–14(i)]. Additions of Cu, Fe, and Ni as solutes result in a CET in DED-LB Ti alloys, but Mo does not. The incorporation of Cu, Fe, and Ni significantly enhances both Q and P, while an increase in Mo content accelerates the rise of Q more dramatically than that of P. ΔT_s was not a reliable parameter for predicting a CET. In PBF-LB, an elevated solidification velocity may affect the extent of solute partitioning due to solute trapping. The findings of Brooke *et al.*[114] aligned closely with historical theories of the CET predicated on dendritic tip undercoolings. Constitutional supercooling driven by solutes is contingent upon the velocity of solidification. At elevated solidification velocities, such as those observed in AM, the undercooling of the dendritic tip is more strongly associated with P, but at lower solidification velocities, typical of casting processes, it correlates more closely with Q. The results provided

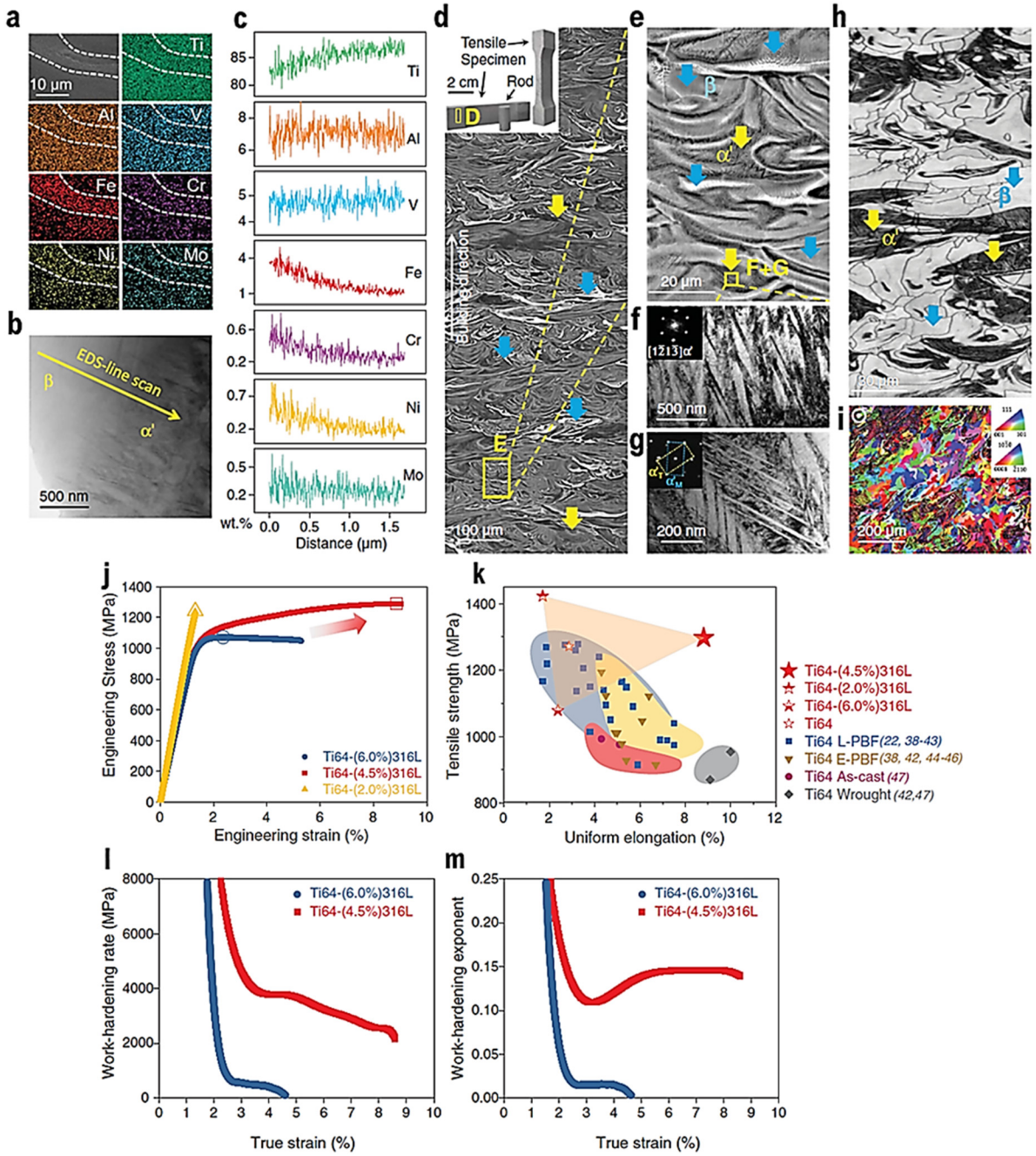

FIG. 12. *In situ* design of advanced AMed Ti alloys through micro-scale concentration modulations (μ-CM) approach. (a) SEM-EDS maps of as-fabricated Ti64–(4.5%) 316L demonstrating micrometer-scale depletion of Ti, Al, and V alongside enrichment of Fe, Cr, and Ni elements inside a specific swirl of the melt pool. (b) S-TEM micrograph depicting the β-α′ interface region alongside the EDS line scan orientation, (c) compositional profiles spanning the β-α′ interphase boundary. Side-view cross section BSE-SEM displays a lava-like microstructure characterized by a distinct swirl pattern. (d) and (e) The SEM-BSE image at low and higher magnifications emphasize the heterogeneous microstructure, featuring the coexistence of acicular α′ martensite and ultrafine β grains alongside a solidification cellular structure. (f) BF-TEM of fine acicular α′ martensite, (g) BF-TEM of ultrafine twin structure, (h) band contrast, and (i) EBSD of as-printed Ti64–(4.5%)316L, (j)–(m) mechanical properties and work-hardening rate curve of the as-fabricated microCM Ti64–x316L alloy, alongside a comparison of tensile properties with Ti64 alloy produced via various AM methods and conventional technologies. Reproduced with permission from Zhang *et al.*, Science **374**, 478 (2021).[112] Copyright 2021 American Association for the Advancement of Science.

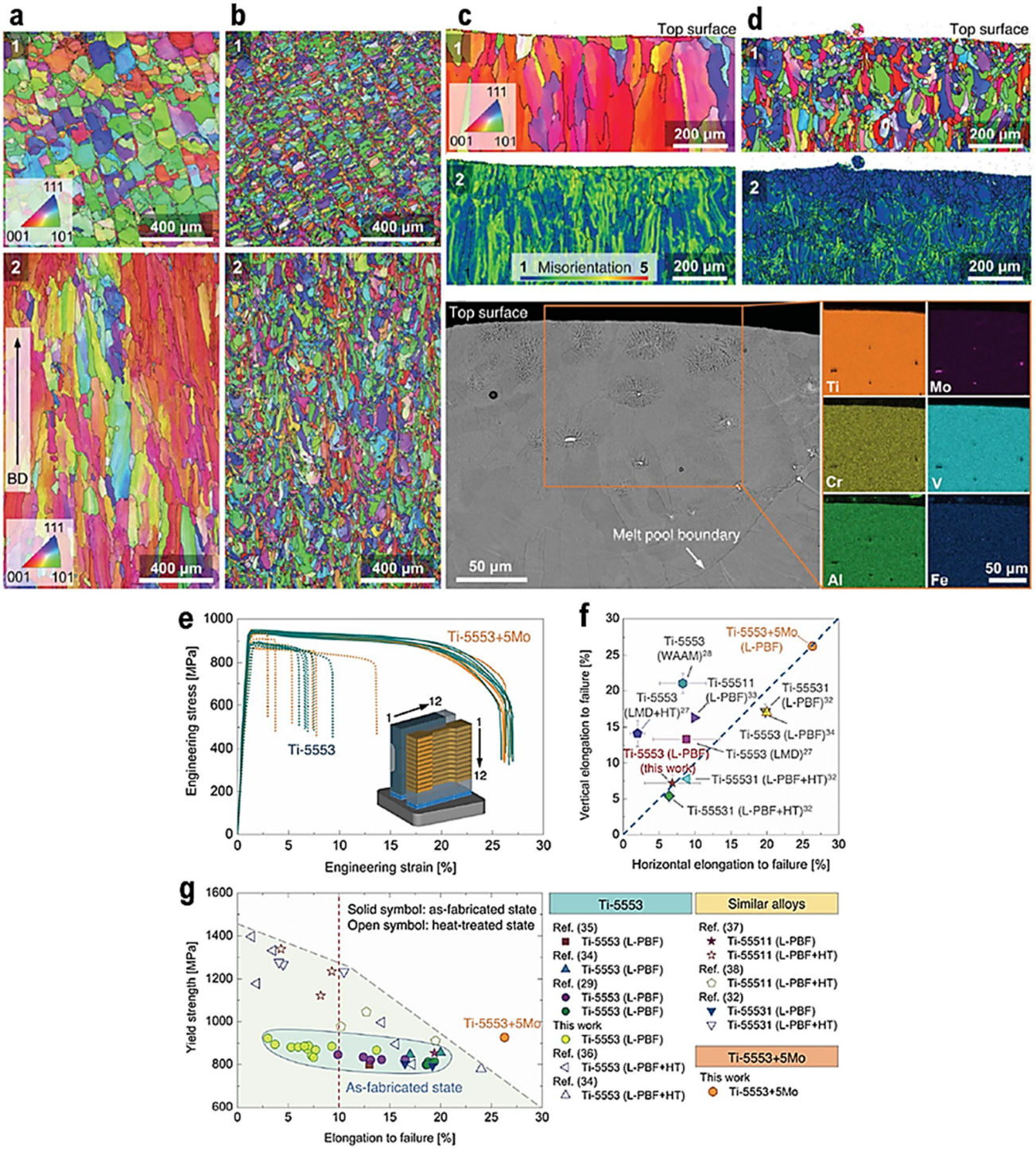

FIG. 13. Exploiting bifunctional alloy design to produce ultra-uniform, strong, and ductile 3D-printed Ti5553 alloy. EBSD-IPF and EBSD-KAM analyses of (a) and (c) Ti-5553 and (b) and (d) Ti-5553 + 5Mo specimens; (e)–(g) tensile engineering stress–strain curves for Ti-5553 and Ti-5553 + 5Mo specimens in vertical and horizontal orientations, compared to Ti-5553, Ti-55531, Ti-55511, and Ti-5553 + 5Mo produced via various 3D-printing techniques, with and without post-printing heat treatment. Reproduced with permission from Zhang *et al.*, Science **383**, 6683 (2024).[113] Copyright 2024 American Association for the Advancement of Science.

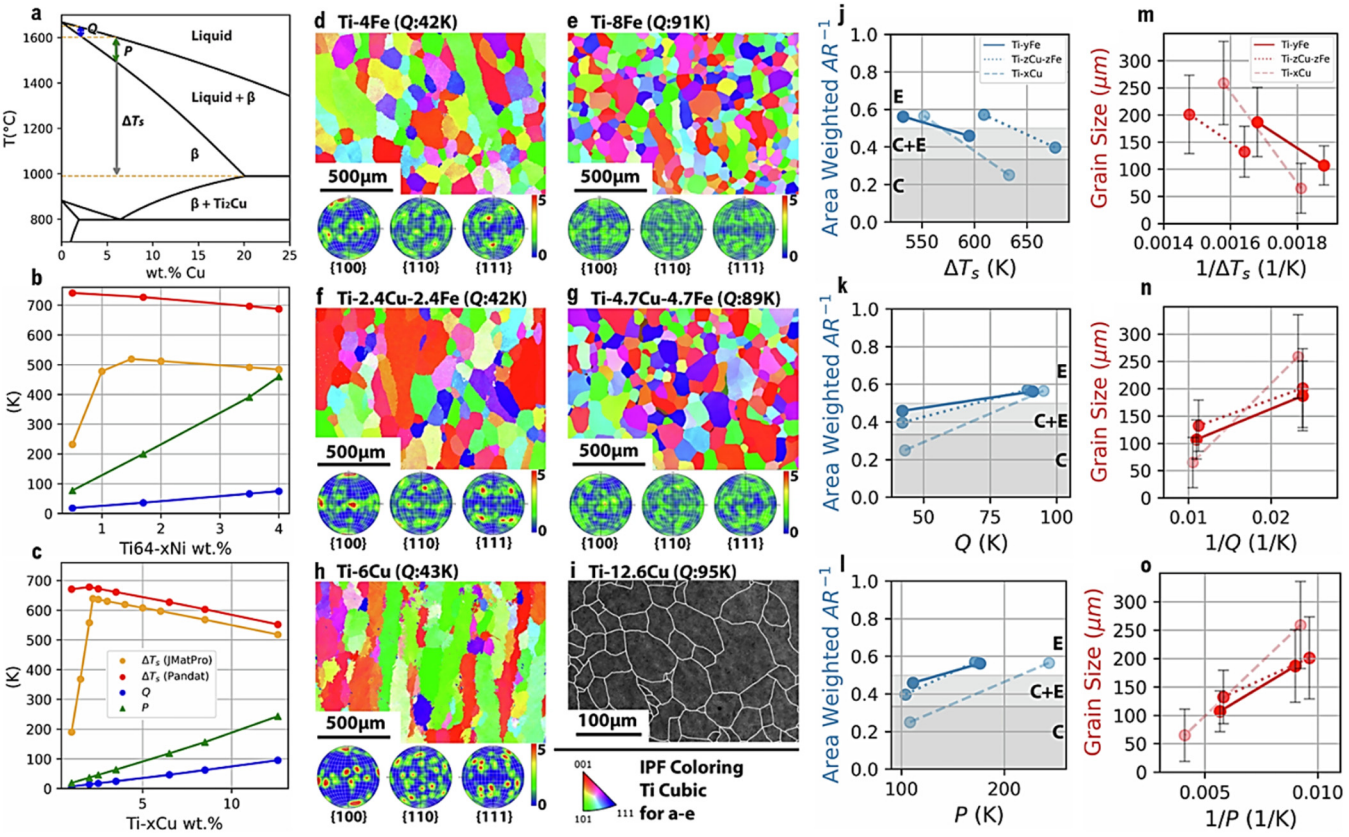

FIG. 14. Compositional criteria for predicting columnar to equiaxed transitions in metal additive manufacturing. (a) The phase diagram depicts the ΔT_s (gray range), Q (blue range), and P (green range) values for Ti–6Cu, (b), (c) The Scheil solidification range (ΔT_s), the growth restriction factor (Q), and the supercooling parameter (P) were calculated for Ti6Al–4V–xNi and Ti–xCu alloys, respectively. For the purpose of comparison, ΔT_s were extracted from two CALPHAD sources: PANDAT TM (PanTi2022 database) and JMatPro (Titanium alloy database). (d) and (e) Ti–Fe, (f) and (g) Ti–Cu–Fe, and (h) and (i) Ti–Cu alloys were produced at growth restriction factors (Q) of approximately 42 and 93 K, respectively. The reconstructed parent β-grains from EBSD data are illustrated in (d)–(h). (i) The BSE image illustrates the traced parent β-grains, which are identified by hyper-eutectoid Ti_2Cu. The magnification of Ti–12.6Cu has been increased (i). The (j), (m) AR^{-1} and grain size of Ti–Cu, Ti–Fe, and Ti–Cu–Fe alloys are calculated as a function of ΔT_s (the Scheil solidification range), (k), (n) Q (the growth restriction factor), and (l), (o) P (the supercooling parameter). Area weighted AR^{-1} regions corresponding to columnar (C) (dark gray, AR > 3), columnar + equiaxed (C + E) (light gray, AR = 2–3), and equiaxed (E) (white, AR < 2) grains are denoted by the shading in (j)–(l). Reproduced with permission from Brooke *et al.*, Nat. Commun. **16**, 5710 (2025).[114] Copyright 2025 Nature; licensed under a Creative Commons Attribution (CC BY) license.

by Brooke *et al.*[114] established a basis for alloy design and microstructural control, which are essential for both existing and developing AM methods.

VI. CONCLUDING REMARKS AND FUTURE OUTLOOK

This review highlights remarkable advancements in 3D-printed Ti alloys, which can lead to the production of damage-tolerant Ti alloys. This development represents a significant departure from implementing already existing Ti alloys, which were historically ideal for conventional manufacturing techniques, including casting and forging. The significant temperature gradients and non-equilibrium solidification associated with additive manufacturing necessitate a comprehensive reassessment of alloy compositions and microstructural control strategies. In addition, the newly proposed feedstock–process–structure–property–performance ($FPSP^2$) paradigm can be introduced as advancement for the conventional process–structure–property (PSP) paradigm. This integrated and efficient approach of materials development explicitly addresses both the features of the feedstock materials and the eventual performance requirements of the AMed component, therefore guiding their development. The novel proposed approaches for microstructural and mechanical development in this review paper revealed that specific alloy design can surpass the existing challenges in AMed Ti alloys, including the fabrication of columnar grains and the resultant anisotropic mechanical properties. The development of nanotwinned precipitates by applying post-AM techniques and the encouragement of grain refinement through the controlled addition of copper were examples of advanced techniques that highlight the ability to control alloy

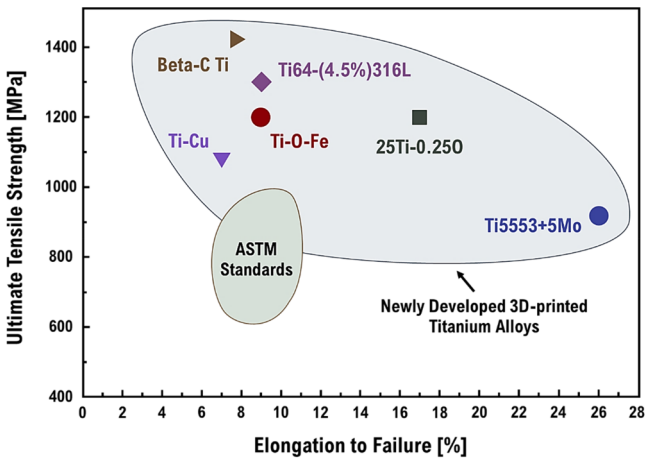

FIG. 15. Ultimate tensile strength and elongation to failure of the newly developed 3D-printed Ti alloys with unique strength-ductility vs conventional ASTM cast and wrought techniques for titanium production.

composition precisely. Moreover, by deliberately incorporating iron and oxygen, one can obtain nano-homogeneity and improve the balance between strength and ductility. The proposed approaches can precisely regulate the microstructure of the AM Ti alloy, therefore altering fundamental features including phase transitions, grain morphologies, and mechanical strength of the resulting components. In Fig. 15, we summarized the ultimate tensile strength and elongation to failure of the recently developed 3D-printed Ti alloys in Sec. V, which exhibited an exceptional strength-ductility as compared to conventional ASTM cast and wrought techniques for Ti production.

The rising complexity of analytical microstructure development models, best shown by the Kurz–Giovanola–Trivedi (KGT) dendrite growth model and the new grain nucleation models derived from the Hunt Columnar-to-Equiaxed Transition (CET) model, offers a potent approach for predicting and controlling grain structure during AM processes. Together with advanced characterization methods including EBSD, TEM, and APT, these models provide insightful analysis of the fundamental processes controlling microstructure evolution and help rationalize Ti alloys with exactly desired properties. Looking ahead, several paramount fields of study deserve concentrated effort to broaden the area of Ti alloy design. Accelerating alloy identification and optimization, especially for AM, somehow depends on combining computational thermodynamics (CALPHAD) and kinetic simulations with machine learning methods. Under AM conditions, we must construct strong and predictive models that correctly predict microstructure and mechanical properties. Concurrently, real-time monitoring of the AM process using advanced sensors and feedback control systems would enable dynamic changes to process parameters, therefore enabling the manufacturing of desired microstructures and features *in situ*. This covers control over temperature gradients, cooling rates, and melt pool dynamics. Furthermore, the rapid solidifications inherent in AM offer the unique possibility to generate novel metastable phases with unparalleled properties, which demands more significant research to understand their genesis and stability and to create strategies for controlling their precipitation and concomitant breakdown. Apart from these developments, the continuous use of AM Ti alloys, depending on established testing requirements and strong qualification processes, guarantees total acceptability in many disciplines. This investigates the evolution of dependable and consistent approaches for evaluating mechanical characteristics, fatigue resistance, and fracture toughness, critical performance criteria. Dealing with the challenges presented by anisotropy remains a top concern; hence, new strategies for obtaining isotropic properties in AM Ti alloys must be developed by alloy design or modification. Furthermore, this review lays the groundwork for developing novel chemically modified Ti-based alloys with tailored properties for various applications.

AUTHOR DECLARATIONS

Conflict of Interest

The authors have no conflicts to disclose.

Author Contributions

Saeid Alipour: Conceptualization (equal); Data curation (equal); Formal analysis (equal); Investigation (equal); Methodology (equal); Writing – original draft (equal); Writing – review & editing (equal). **Arezoo Emdadi:** Conceptualization (equal); Supervision (equal); Validation (equal); Visualization (equal); Writing – original draft (equal); Writing – review & editing (equal). **Ju Li:** Conceptualization (equal); Methodology (equal); Project administration (equal); Supervision (equal); Validation (equal); Visualization (equal); Writing – original draft (equal); Writing – review & editing (equal).

DATA AVAILABILITY

Data sharing is not applicable to this article as no new data were created in this study.

REFERENCES

[1] ASTM-F2792, "Standard terminology for additive manufacturing technologies," ASTM Int. **46**, 10.04 (2012).
[2] A. A. Shapiro *et al.*, "Additive manufacturing for aerospace flight applications," J. Spacecr. Rock. **53**, 952–959 (2016).
[3] V. Mohanavel *et al.*, "The roles and applications of additive manufacturing in the aerospace and automobile sector," Mater. Today: Proc. **47**, 405–409 (2021).
[4] C. Sun *et al.*, "Additive manufacturing for energy: A review," Appl. Energy **282**, 116041 (2021).
[5] A. Zhakeyev *et al.*, "Additive manufacturing: Unlocking the evolution of energy materials," Adv. Sci. **4**(10), 1700187 (2017).
[6] M. Sarraf *et al.*, "A state-of-the-art review of the fabrication and characteristics of titanium and its alloys for biomedical applications," Bio-Des. Manuf. **5**, 371–395 (2022).
[7] S. Alipour *et al.*, "A review on *in vitro*/*in vivo* response of additively manufactured Ti-6Al-4V alloy," J. Mater. Chem. B **10**(46), 9479–9534 (2022).

[8]S. Alipour *et al.*, "The trajectory of additively manufactured titanium alloys with superior mechanical properties and engineered microstructures," Addit. Manuf. **60**, 103245 (2022).
[9]B. Dutta and F. H. S. Froes, *The Additive Manufacturing (AM) of Titanium Alloys, in Titanium Powder Metallurgy* (Elsevier, 2015), pp. 447–468.
[10]D. Rabbitt *et al.*, "Rethinking biomedical titanium alloy design: A review of challenges from biological and manufacturing perspectives," Adv. Healthcare Mater. **14**(4), 2403129 (2025).
[11]R. Mahamood and E. T. Akinlabi, "Corrosion behavior of laser additive manufactured titanium alloy," Int. J. Adv. Manuf. Technol. **99**, 1545–1552 (2018).
[12]T. S. Tshephe *et al.*, "Additive manufacturing of titanium-based alloys—A review of methods, properties, challenges, and prospects," Heliyon **8**(3), e09041 (2022).
[13]E. Uhlmann *et al.*, "Additive manufacturing of titanium alloy for aircraft components," Proc. CIRP **35**, 55–60 (2015).
[14]S. Rawal, J. Brantley, and N. Karabudak, "Additive manufacturing of Ti-6Al-4V alloy components for spacecraft applications," in *2013 6th International Conference on Recent Advances in Space Technologies (RAST)* (IEEE, 2013).
[15]P. Nyamekye *et al.*, "Impact of additive manufacturing on titanium supply chain: Case of titanium alloys in automotive and aerospace industries," Adv. Ind. Manuf. Eng. **6**(C), 100112 (2023).
[16]M. A. Mahmood *et al.*, "Post-processing techniques to enhance the quality of metallic parts produced by additive manufacturing," Metals **12**(1), 77 (2022).
[17]M. Qian *et al.*, "Additive manufacturing and postprocessing of Ti-6Al-4V for superior mechanical properties," MRS Bull. **41**(10), 775–784 (2016).
[18]Z. Zhang *et al.*, "Achieving grain refinement and enhanced mechanical properties in Ti-6Al-4V alloy produced by multidirectional isothermal forging," Mater. Sci. Eng. A **692**, 127–138 (2017).
[19]J. Bustillos, J. Kim, and A. Moridi, "Exploiting lack of fusion defects for microstructural engineering in additive manufacturing," Addit. Manuf. **48**, 102399 (2021).
[20]A. Basak and S. Das, "Epitaxy and microstructure evolution in metal additive manufacturing," Annu. Rev. Mater. Res. **46**(1), 125–149 (2016).
[21]S. Chandra *et al.*, "Solidification in metal additive manufacturing: Challenges, solutions, and opportunities," Prog. Mater. Sci. **148**, 101361 (2024).
[22]A. Mostafaei *et al.*, "Defects and anomalies in powder bed fusion metal additive manufacturing," Curr. Opin. Solid State Mater. Sci. **26**(2), 100974 (2022).
[23]K.-H. Jin *et al.*, "Achieving enhanced tensile strength-ductility synergy through phase modulation in additively manufactured titanium alloys," Mater. Sci. Eng. A **909**, 146801 (2024).
[24]M. Zang *et al.*, "Achieving highly promising strength-ductility synergy of powder bed fusion additively manufactured titanium alloy components at ultra-low temperatures," Addit. Manuf. **65**, 103444 (2023).
[25]T. Wang *et al.*, "Laser additive manufacturing of new α + β titanium alloy with high strength and ductility," J. Mater. Res. Technol. **26**, 7566–7582 (2023).
[26]X. Pang *et al.*, "Enhanced strength-ductility synergy in laser additive manufactured TC4 titanium alloy by grain refinement," Mater. Lett. **326**, 132949 (2022).
[27]P. Wang *et al.*, "Deformation induced nanoscale twinning improves strength and ductility in additively manufactured titanium alloys," Mater. Sci. Eng. A **833**, 142568 (2022).
[28]C. Zhou *et al.*, "Simultaneously achieving strength-ductility in additive-manufactured Ti6Al4V alloy via ultrasonic surface rolling process," Mater. Sci. Eng. A **920**, 147555 (2025).
[29]D. Yuan *et al.*, "Grain refining of Ti-6Al-4V alloy fabricated by laser and wire additive manufacturing assisted with ultrasonic vibration," Ultrason. Sonochem. **73**, 105472 (2021).
[30]A. I. Gorunov, "Additive manufacturing of Ti6Al4V parts using ultrasonic assisted direct energy deposition," J. Manuf. Process. **59**, 545–556 (2020).
[31]A. Zafari and K. Xia, "Superior titanium from hybridised microstructures—A new strategy for future alloys," Scr. Mater. **173**, 61–65 (2019).
[32]A. Zafari *et al.*, "Overcoming strength-ductility trade-off by hybridising different classes of titanium alloys," Mater. Sci. Eng. A **922**, 147613 (2025).
[33]W. Xu *et al.*, "*In situ* tailoring microstructure in additively manufactured Ti-6Al-4V for superior mechanical performance," Acta Mater. **125**, 390–400 (2017).
[34]J. Lv *et al.*, "Achieving high strength and ductility in selective laser melting Ti-6Al-4V alloy by laser shock peening," J. Alloys Compd. **899**, 163335 (2022).
[35]M. Knezevic *et al.*, "Thermo-hydrogen refinement of microstructure to improve mechanical properties of Ti-6Al-4V fabricated via laser powder bed fusion," Mater. Sci. Eng. A **809**, 140980 (2021).
[36]M. N. Doğu *et al.*, "Microstructural and texture evolution during thermo-hydrogen processing of Ti6Al4V alloys produced by electron beam melting," Mater. Charact. **168**, 110549 (2020).
[37]A. E. Davis *et al.*, "The effect of processing parameters on rapid-heating β recrystallization in inter-pass deformed Ti-6Al-4V wire-arc additive manufacturing," Mater. Charact. **163**, 110298 (2020).
[38]X. Guo *et al.*, "Wire-arc directed energy deposition of Ti-6Al-4V alloy using CO_2 active interpass cooling: Phase composition, grain orientation, texture strength, dislocation density and mechanical property," J. Mater. Res. Technol. **28**, 3196–3206 (2024).
[39]X. Tian *et al.*, "Isotropic and improved tensile properties of Ti-6Al-4V achieved by in-situ rolling in direct energy deposition," Addit. Manuf. **46**, 102151 (2021).
[40]Y. Fu *et al.*, "Optimization of shape and performance for wire and arc additive manufacturing with in-situ rolling of Ti-6Al-4V ELI alloy," J. Mater. Res. Technol. **35**, 4833 (2025).
[41]J. Kennedy *et al.*, "Isomorphic grain inoculation in Ti-6Al-4V during additive manufacturing," Mater. Lett.: X **8**, 100057 (2020).
[42]J. R. Kennedy *et al.*, "The potential for grain refinement of wire-arc additive manufactured (WAAM) Ti-6Al-4V by ZrN and TiN inoculation," Addit. Manuf. **40**, 101928 (2021).
[43]D. H. St John *et al.*, "The challenges associated with the formation of equiaxed grains during additive manufacturing of titanium alloys," Key Eng. Mater. **770**, 155–164 (2018).
[44]M. Syverud, T. Okabe, and H. Herø, "Casting of TI-6AI-4V alloy compared with pure Ti in an Ar-arc casting machine," Eur. J. Oral Sci. **103**(5), 327–330 (1995).
[45]C. Hickey, Jr. and T. DeSisto, *Mechanical Properties and Fracture Toughness of Ti-6Al-2Sn-4Zr-2Mo* (Army Materials and Mechanics Research Center, Watertown, MA, 1973).
[46]S. Veeck, D. Lee. R. Boyer, and R. Briggs, "The castability of Ti-5553 alloy: Its microstructure and properties," J. Adv. Mater. **37**(4), 40–45 (2005).
[47]P. Pushp, S. Dasharath, and C. Arati, "Classification and applications of titanium and its alloys," Mater. Today: Proc. **54**, 537–542 (2022).
[48]M. Najafizadeh *et al.*, "Classification and applications of titanium and its alloys: A review," J. Alloys Comps. Commun. **3**, 100019 (2024).
[49]S. R. Soundararajan *et al.*, *Titanium Alloys* (Modern Topics, Welding, 2021), p. 203.
[50]T. Ahmed and H. Rack, "Phase transformations during cooling in α + β titanium alloys," Mater. Sci. Eng. A **243**(1–2), 206–211 (1998).
[51]V. Anil Kumar *et al.*, "Recent advances in processing of titanium alloys and titanium aluminides for space applications: A review," J. Mater. Res. **36**, 689–716 (2021).
[52]S. S. Sidhu, H. Singh, and M. A.-H. Gepreel, "A review on alloy design, biological response, and strengthening of β-titanium alloys as biomaterials," Mater. Sci. Eng.: C **121**, 111661 (2021).
[53]P. Omoniyi, E. Akinlabi, and R. Mahamood, "Heat treatments of Ti6Al4V alloys for industrial applications: An overview," in *IOP Conference Series: Materials Science and Engineering* (IOP Publishing, 2021).
[54]R. Cottam *et al.*, "Diffraction line profile analysis of 3D wedge samples of Ti-6Al-4V fabricated using four different additive manufacturing processes," Metals **9**(1), 60 (2019).
[55]Y. Xiong *et al.*, "Data-driven design space exploration and exploitation for design for additive manufacturing," J. Mech. Des. **141**(10), 101101 (2019).
[56]N. Kouraytem *et al.*, "Modeling process–structure–property relationships in metal additive manufacturing: A review on physics-driven versus data-driven approaches," J. Phys. Mater. **4**(3), 032002 (2021).

[57]B. M. Richter and E. H. Glaessgen, "Additive manufacturing (AM) process-structure-property (PSP) frameworks," in *ModSim Ambassadors Program* (NASA, 2022).
[58]R. N. Saunders, "Metal additive manufacturing process-structure-property relational linkages using Gaussian process surrogates," Addit. Manuf. **62**, 103398 (2023).
[59]C. Fredriksson, "Sustainability of metal powder additive manufacturing," Proc. Manuf. **33**, 139–144 (2019).
[60]R. Sreenivasan, A. Goel, and D. L. Bourell, "Sustainability issues in laser-based additive manufacturing," Phys. Proc. **5**, 81–90 (2010).
[61]J. Baskaran, "Roadmap to achieve sustainable and eco-friendly metal additive manufacturing processes," in *Futuristic Technology for Sustainable Manufacturing* (IGI Global, 2024), pp. 185–215.
[62]H. Eskandari *et al.*, "Microstructural characterization and mechanical properties of SLM-printed Ti-6Al-4V alloy: Effect of build orientation," J. Mater. Res. **37**(16), 2645–2660 (2022).
[63]S. Skvortsova, M. German, and V. Spektor, "Structure and properties of alloy Ti-6Al-4V samples fabricated by 3D printing," Russ. Metall. **2019**, 863–872.
[64]M. Bermingham *et al.*, "Promoting the columnar to equiaxed transition and grain refinement of titanium alloys during additive manufacturing," Acta Mater. **168**, 261–274 (2019).
[65]J. Wang *et al.*, "Columnar-to-equiaxed transition mechanism and remarkable strengthening effect in additive manufactured pure titanium induced by copper addition," Mater. Charact. **209**, 113750 (2024).
[66]M. M. Kirka *et al.*, "Strategy for texture management in metals additive manufacturing," JOM **69**, 523–531 (2017).
[67]F. Arias-González *et al.*, "Microstructure and crystallographic texture of pure titanium parts generated by laser additive manufacturing," Met. Mater. Int. **24**, 231–239 (2018).
[68]Y.-Y. Zhu *et al.*, "Solidification behavior and grain morphology of laser additive manufacturing titanium alloys," J. Alloys Compd. **777**, 712–716 (2019).
[69]S. Suwas and R. Vikram, "Texture evolution in metallic materials during additive manufacturing: A review," Trans. Ind. Natl. Acad. Eng. **6**(4), 991–1003 (2021).
[70]H. Z. Fu and L. Liu, "Progress of directional solidification in processing of advanced materials," in *Materials Science Forum* (Trans Tech Publications, 2005).
[71]M. Simonelli, Y. Y. Tse, and C. Tuck, "On the texture formation of selective laser melted Ti-6Al-4V," Metall. Mater. Trans. A **45**, 2863–2872 (2014).
[72]S. Tekumalla *et al.*, "Towards 3-D texture control in a β titanium alloy via laser powder bed fusion and its implications on mechanical properties," Addit. Manuf. **59**, 103111 (2022).
[73]S. Alipour *et al.*, "Implementation of miniature tensile specimens in mechanical properties assessment of directed energy deposited Ti-6Al-4V: As-built and heat treated," Mater. Sci. Eng. A **921**, 147593 (2025).
[74]W. Kurz, B. Giovanola, and R. Trivedi, "Theory of microstructural development during rapid solidification," Acta Metall. **34**(5), 823–830 (1986).
[75]A. T. Polonsky, *Three-Dimensional Characterization of Additively Manufactured Metals* (University of California, Santa Barbara, 2020).
[76]W. J. Boettinger *et al.*, "Solidification microstructures: Recent developments, future directions," Acta Mater. **48**(1), 43–70 (2000).
[77]X. Wang and W. Xiong, "Uncertainty quantification and composition optimization for alloy additive manufacturing through a CALPHAD-based ICME framework," npj Comput. Mater. **6**(1), 188 (2020).
[78]Z. Liang *et al.*, "Development of computational framework for titanium alloy phase transformation prediction in laser powder-bed fusion additive manufacturing," Materialia **14**, 100934 (2020).
[79]R. Jha and G. S. Dulikravich, "Discovery of new Ti-based alloys aimed at avoiding/minimizing formation of α" and ω-phase using CALPHAD and artificial intelligence," Metals **11**(1), 15 (2021).
[80]M. Assi, *Alloys Design for Additive Manufacturing (ADAM)* (Ecole Nationale Supérieure des Mines de Saint-Etienne, 2022).
[81]A. Roy *et al.*, "Columnar-to-equiaxed transition in laser fusion additive manufacturing," Scr. Mater. **259**, 116565 (2025).
[82]P. Mohammadpour, A. Plotkowski, and A. B. Phillion, "Revisiting solidification microstructure selection maps in the frame of additive manufacturing," Addit. Manuf. **31**, 100936 (2020).
[83]A. Davis *et al.*, "Achieving a columnar-to-equiaxed transition through dendrite twinning in high deposition rate additively manufactured titanium alloys," Metall. Mater. Trans. A **55**(6), 1765–1787 (2024).
[84]J. Spittle, "Columnar to equiaxed grain transition in as solidified alloys," Int. Mater. Rev. **51**(4), 247–269 (2006).
[85]D. Pineda and M. A. Martorano, "Columnar to equiaxed transition in directional solidification of inoculated melts," Acta Mater. **61**(5), 1785–1797 (2013).
[86]M. Wu and A. Ludwig, "Using a three-phase deterministic model for the columnar-to-equiaxed transition," Metall. Mater. Trans. A **38**, 1465–1475 (2007).
[87]M. A. Martorano and V. B. Biscuola, "Predicting the columnar-to-equiaxed transition for a distribution of nucleation undercoolings," Acta Mater. **57**(2), 607–615 (2009).
[88]M. Gäumann, R. Trivedi, and W. Kurz, "Nucleation ahead of the advancing interface in directional solidification," Mater. Sci. Eng. A **226–228**, 763–769 (1997).
[89]M. Seredyński, M. Rebow, and J. Banaszek, "The role of the dendritic growth model dimensionality in predicting the columnar to equiaxed transition (CET)," Heat Mass Transfer **54**(8), 2581–2588 (2018).
[90]M. Gaumann and W. Kurz, "Why is it so difficult to produce an equiaxed microstructure during welding?," in *Mathematical Modelling of Weld Phenomena: No. 4* (CRC Press, 2024), pp. 125–136.
[91]Z. Fan *et al.*, "Effect of solutes on grain refinement," Prog. Mater. Sci. **123**, 100809 (2022).
[92]J. Wang *et al.*, "Grain morphology evolution and texture characterization of wire and arc additive manufactured Ti-6Al-4V," J. Alloys Compd. **768**, 97–113 (2018).
[93]M. Gäumann *et al.*, "Single-crystal laser deposition of superalloys: Processing–microstructure maps," Acta Mater. **49**(6), 1051–1062 (2001).
[94]M. Y. Mendoza *et al.*, "Microstructures and grain refinement of additive-manufactured Ti–xW alloys," Metall. Mater. Trans. A **48**, 3594–3605 (2017).
[95]X. Wang *et al.*, "Hierarchical grain refinement during the laser additive manufacturing of Ti-6Al-4V alloys by the addition of micron-sized refractory particles," Addit. Manuf. **45**, 102045 (2021).
[96]Z. Fan and F. Gao, "Grain initiation and grain refinement: An overview," Metals **12**(10), 1728 (2022).
[97]D. M. Stefanescu, *Cellular and Dendritic Growth, in Science and Engineering of Casting Solidification*, 2nd ed. (Springer, 2008), pp. 1–38.
[98]J. Yoshioka and M. Eshraghi, "Temporal evolution of temperature gradient and solidification rate in laser powder bed fusion additive manufacturing," Heat Mass Transfer **59**(7), 1155–1166 (2023).
[99]W. Ou *et al.*, "Fusion zone geometries, cooling rates and solidification parameters during wire arc additive manufacturing," Int. J. Heat Mass Transfer **127**, 1084–1094 (2018).
[100]V. Manvatkar, A. De, and T. DebRoy, "Spatial variation of melt pool geometry, peak temperature and solidification parameters during laser assisted additive manufacturing process," Mater. Sci. Technol. **31**(8), 924–930 (2015).
[101]M. M. Kirka *et al.*, "Solidification and solid-state transformation sciences in metals additive manufacturing," Scr. Mater. **135**, 130–134 (2017).
[102]Z. Wang *et al.*, "Optimization of processing parameters and establishment of a relationship between microstructure and mechanical properties of SLM titanium alloy," Opt. Laser Technol. **112**, 159–167 (2019).
[103]H. Gong *et al.*, "The effects of processing parameters on defect regularity in Ti–6Al–4V parts fabricated by selective laser melting and electron beam melting," in *24th Annual International Solid Freeform Fabrication Symposium* (University of Texas at Austin, 2013).
[104]H. Kim, Y. Lin, and T.-L. B. Tseng, "A review on quality control in additive manufacturing," Rapid Prototyp. J. **24**(3), 645–669 (2018).
[105]J. P. Oliveira, A. LaLonde, and J. Ma, "Processing parameters in laser powder bed fusion metal additive manufacturing," Mater. Des. **193**, 108762 (2020).

[106]D. Zhang *et al.*, "Additive manufacturing of ultrafine-grained high-strength titanium alloys," Nature **576**(7785), 91–95 (2019).
[107]T. Song *et al.*, "Strong and ductile titanium–oxygen–iron alloys by additive manufacturing," Nature **618**(7963), 63–68 (2023).
[108]Y. Zhu *et al.*, "Ultrastrong nanotwinned titanium alloys through additive manufacturing," Nat. Mater. **21**(11), 1258–1262 (2022).
[109]J. Zhang *et al.*, "Designing against phase and property heterogeneities in additively manufactured titanium alloys," Nat. Commun. **13**(1), 4660 (2022).
[110]M. S. Nartu *et al.*, "Underlying factors determining grain morphologies in high-strength titanium alloys processed by additive manufacturing," Nat. Commun. **14**(1), 3288 (2023).
[111]P. Barriobero-Vila *et al.*, "Peritectic titanium alloys for 3D printing," Nat. Commun. **9**(1), 3426 (2018).
[112]T. Zhang *et al.*, "*In situ* design of advanced titanium alloy with concentration modulations by additive manufacturing," Science **374**(6566), 478–482 (2021).
[113]J. Zhang *et al.*, "Ultrauniform, strong, and ductile 3D-printed titanium alloy through bifunctional alloy design," Science **383**(6683), 639–645 (2024).
[114]R. Brooke *et al.*, "Compositional criteria to predict columnar to equiaxed transitions in metal additive manufacturing," Nat. Commun. **16**(1), 5710 (2025).